iScience

CellPress
OPEN ACCESS

Article

Expression of nonmuscle myosin IIC is regulated by non-canonical binding activity of miRNAs

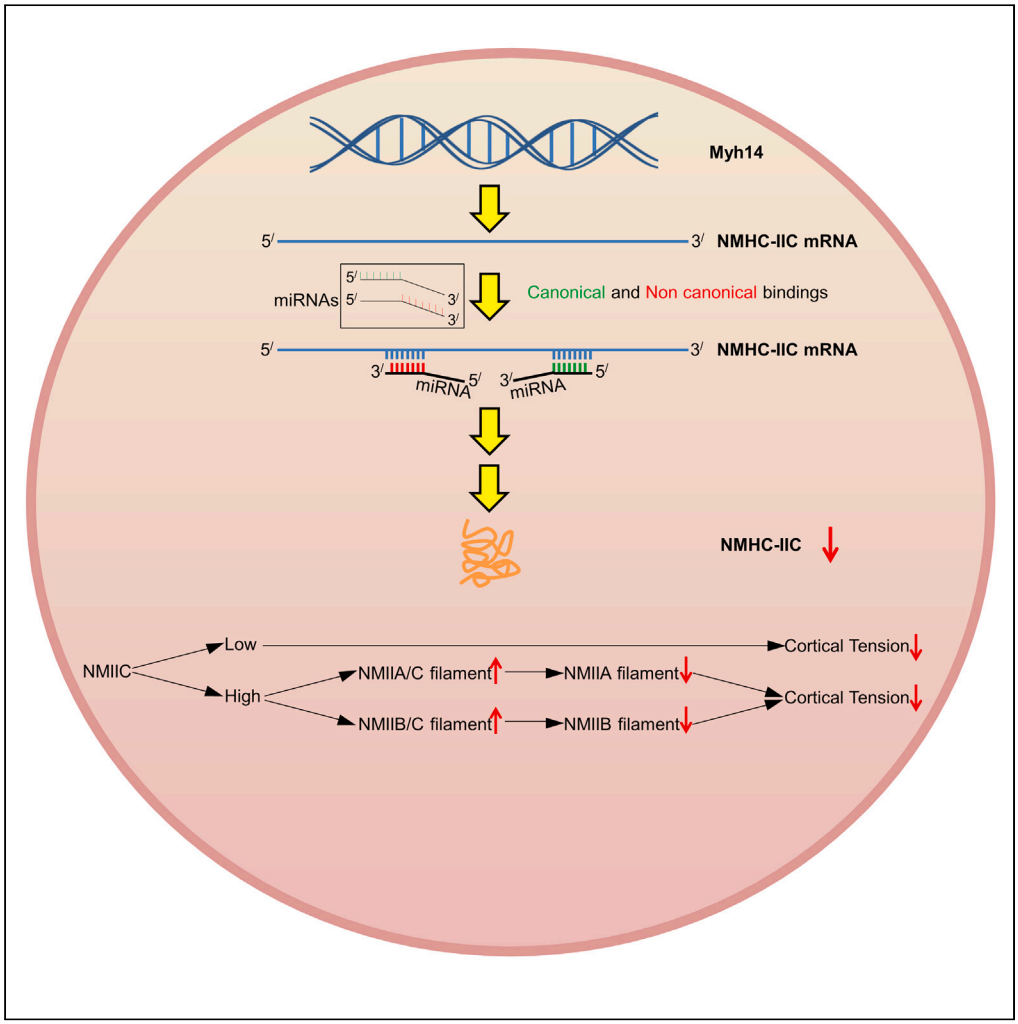

Kumarjeet Banerjee, Shekhar Saha, Shaoli Das, Suman Ghosal, Indranil Ghosh, Abhimanyu Basu, Siddhartha S. Jana

bcssj@iacs.res.in

Highlights

Expression of nonmuscle myosin IIC (NMIIC) can be regulated by miRNAs

Non canonical bindings of miRNAs add the efficacy of canonical bindings

Heterofilament formation of NMIIC with NMIIA and -IIB regulate cortical tension in cell

Banerjee et al., iScience *26*, 108384
December 15, 2023 © 2023
https://doi.org/10.1016/j.isci.2023.108384

iScience

CellPress
OPEN ACCESS

Article

Expression of nonmuscle myosin IIC is regulated by non-canonical binding activity of miRNAs

Kumarjeet Banerjee,[1] Shekhar Saha,[2] Shaoli Das,[3] Suman Ghosal,[4] Indranil Ghosh,[1] Abhimanyu Basu,[5] and Siddhartha S. Jana[1,6,*]

SUMMARY

The expression of mechanoresponsive nonmuscle myosin II (NMII)C is found to be inducible during tumor progression, but its mechanism is yet to be explored. Here, we report a group of microRNAs (mmu-miR-200a-5p, mmu-miR-532-3p, mmu-miR-680, and mmu-miR-1901) can significantly repress the expression of nonmuscle myosin IIC (NMIIC). Interestingly, these microRNAs have both canonical and non-canonical binding sites at 3′UTR and coding sequence (CDS) of NMIIC's heavy chain (HC) mRNA. Each of the miRNA downregulates NMHC-IIC to a different degree as assessed by dual-luciferase and immunoblot analyses. When we abolish the complementary base pairing at canonical binding site, mmu-miR-532-3p can still bind at non-canonical binding site and form Argonaute2 (AGO2)-miRNA complex to downregulate the expression of NMIIC. Modulating the expression of NMIIC by miR-532-3p in mouse mammary tumor cells, 4T1, increases its tumorigenic potential both *in vitro* and *in vivo*. Together, these studies provide the functional role of miRNA's non-canonical binding mediated NMIIC regulation in tumor cells.

INTRODUCTION

Recent studies estimate that approximately 30% of expressed transcripts in human are regulated by endogenous miRNAs.[1] miRNAs are a class of non-coding RNAs that are ~22 nucleotides in length and can interact with mRNA, tRNA and even lncRNA. Their interactions with target molecules are thought to be mediated through the canonical and non-canonical "seed sites."[2,3] The miRNA-mRNA base-pairing interaction has been shown to determine the degree of target repression.[4] Hausser et al.[5] have demonstrated that complementary sites at coding sequence (CDS) are most potent in inhibiting translation while those at 3′UTR are more efficient in triggering mRNA degradation. Besides the conventional (canonical) seed region i.e., 5′end of miRNA (base position 2–7 or 2–8) other types of miRNA target sites including bulges in the seed position and complementary sites from 3′end of miRNA play important role in miRNA-target interactions.[3,6] Interestingly, recent studies showed that numerous genes which encode miRNAs are located within genomic regions are linked to cancer, and changes in these genes, whether through genetic mutations, epigenetic suppression, or abnormalities, can lead to unusual miRNA expression. These differentially expressed miRNAs influence cell survival, growth, and proliferation in diverse cells or tissues in distinct ways.[7–10]

Regulation of actin binding motor protein, nonmuscle myosin II (NMII) by endogenous miRNA is not well explored. The hexameric NMIIs, which are composed of each pair of heavy chains (HCs), regulatory light chains (RLCs), and essential light chains (ELCs), involve in many key cellular processes such as cytokinesis, adhesion and migration.[11–14] To date, three paralogs of NMIIs, NMIIA, IIB, and IIC, based on their heavy chains' similarity have been identified in mammals. The heavy chains are encoded by three different genes, MYH9, MYH10, and MYH14, located on three different chromosomes.[13,14] NMII activity can be regulated by multiple factors such as regulatory light chain kinases, myosin light-chain kinase (MLCK) and ROCK by changing the assembly and actin activated Mg ATPase activity,[13–15] and HC kinases, PKC, CKII, and TRPM7 and tail domain binding protein, S100A4, UNC45a, and Lgl-1 by changing the assembly and disassembly dynamics.[16–18] Also, factors like D39, a derivative of ophiopogon saponin, can inhibit the expression of tissue factors by binding to NMHC-IIA and Ginsenoside Rg1, suppress the secretion of miRNAs from exosomes by inhibiting the interaction between NMHC-IIA and HSP90 in macrophages have been demonstrated to regulate NMII's function.[19,20] Recently, various miRNAs have been shown to modulate NMII indirectly by targeting its several upstream regulators or directly by targeting its heavy chains. MiR-155, miR-374a, and miR-106-363 can target MLCK and MLCK-interacting protein, respectively,[21–23] whereas miR-23b and miR-200c have been found to modulate the phosphorylation of RLC by targeting p-21 activated kinase2 (PAK2) and serum responsive factor (SRF) respectively.[24,25] On the other hand, miRNA, let-7f directly binds to the 3′UTR of MYH9 (NMHC-IIA) in rectal cancer HCT116 cells,[26,27] and hsa-miR-181a-5p and hsa-miR-200a-3p bind to 3′UTR of MYH10 (NMHC-IIB) in

[1]School of Biological Sciences, Indian Association for the Cultivation of Science, Kolkata, India
[2]Department of Microbiology, Immunology, and Cancer Biology, Charlottesville, VA, USA
[3]Center for Cancer Research, National Cancer Institute, Bethesda, MD, USA
[4]Bioinformatics and Computational Biosciences Branch, National Institute of Allergy and Infectious Diseases, Bethesda, MD, USA
[5]Department of General Surgery, Institute of Post Graduate Medical Education and Research, Kolkata, India
[6]Lead contact
*Correspondence: bcssj@iacs.res.in
https://doi.org/10.1016/j.isci.2023.108384

This is an open access article under the CC BY-NC-ND license (http://creativecommons.org/licenses/by-nc-nd/4.0/).

Table 1. Predicted miRNAs against NMHC IIC mRNA

Target Gene name	miRNA (*M. musculus*)	Target site at NMHC IIC mRNA	miRNA seed position	miRepress score
Myh14	miR-1901	3′ UTR and ORF	5′ end (c) and 3′ end (nc)	0.75
	miR-680	3′ UTR and ORF	5′ end (c) and 3′ end (nc)	0.74
	miR-200a-5p	3′ UTR and ORF	5′ end (c) and 3′ end (nc)	0.74
	miR-532-3p	3′ UTR and ORF	5′ end (c) and 3′ end (nc)	0.73
	miR-99a	ORF	3′ end (nc)	0.72
	miR-212-3p	ORF	3′ end (nc)	0.72
	miR-712-3p	ORF	3′ end (nc)	0.72
	miR-343	ORF	3′ end (nc)	0.72
	miR-20a	3′ UTR and ORF	5′ end (c)	0.71
	miR-106b	3′ UTR and ORF	5′ end (c)	0.71
	miR-615-3p	3′ UTR and ORF	3′ end (nc)	0.71
	miR-1894-5p	ORF	5′ end (c) and 3′ end (nc)	0.6

miRepress is used to predict the miRNAs targeting NMHC IIC mRNA. The enlisted twelve miRNAs possess miRepress score ≥0.6. c, canonical; nc, non-canonical.

breast cancer MCF-7 cells and in meningioma cells, SF3061/SF4068, respectively.[28,29] But, whether the MYH14 (NMHC-IIC) is regulated by miRNA is not known though the upregulation and downregulation of MYH14 have been reported in different types of cancer.[30–32] Recently, Surcel et al.[33] have shown that the over-expression or knockdown of NMIIC resulted in overall reduction in the cortical tension of Panc10.05 cells, aiding cancer dissemination, suggesting that deregulation of NMIIC enhances tumorigenicity. *In silico* study by Pérez-Valencia et al.[34] suggest that NMIIC, β-catenin, and vimentin can be inter-connected and, it is of great interest to investigate how the low abundance mechanoresponsive NMIIC's expression is regulated in cancer cells.

In this study, we show that several miRNAs can regulate the expression of NMIIC through the complementary pairing at non-canonical and canonical binding regions with 3′UTR and CDS of MYH14. Mimics or inhibitors of these miRNAs increase the growth and migration of mouse breast cancer cells, 4T1, both *in vitro* and *in vivo*, suggesting the importance of both non-canonical and canonical binding regions of miRNAs in maintaining the amount of NMIIC in cancer cells.

RESULTS

miRNAs repress the expression of NMIIC

Previous studies documented that the expression of NMHC-IIC was inducible during tumor progression.[33] We aimed to investigate if miRNAs can regulate the expression of NMHC-IIC. We used our previously published miRepress software[28] for predicting miRNAs which can target NMHC-IIC. miRepress allows searching for miRNA targets with canonical (pairing with the 5′end of miRNA) as well as non-canonical (pairing with the 3′end of miRNA) binding sites at 3′UTR and CDS of NMHC-IICmRNA. Table 1 shows the list of twelve potential miRNAs with miRepress score value ≥ 0.6. We selected the top four miRNAs, mmu-miR-200a-5p, -532-3p, - 680, and -1901, whose miRepress score values were ≥0.73 and possessed both canonical and non-canonical binding regions with NMHC-IICmRNA. Note that all the four miRNAs have multiple binding sites at NMHC-IICmRNA (Table 2) but, they do not have binding site on other paralogs, NMHC-IIA or NMHC-IIB mRNAs. Besides their common target NMHC-IICmRNA, miRepress predicted other mRNAs which can be targeted by miR-200a-5p, miR-532-3p, miR-1901, and miR-680 (Figure 1A). The neural network shows that all these targeted genes, which are involved in various cellular functions like transcriptional regulation and RNA metabolism as assessed by gene ontology biological process enrichment analysis (-log10p > 3.5, Figure 1B), could be affected by these four predicted miRNAs.

We validated their ability to repress NMHC-IIC in cells. We prepared plasmid DNAs encoding GFP-tagged CDS and luciferase tagged 3′UTR of NMHC-IICmRNA to assess the relative importance of binding sites located at CDS and 3′UTR, respectively (Figure 2A). First, we co-transfected luciferase tagged 3′UTR plasmid DNA and each of the mimic miRNAs or their inhibitors (anti-miRNA oligos) in mouse 4T1 cells, and measured the firefly luciferase activity. Figures 2B and 2C shows that luciferase activities in mimic mRNA transfected cells were significantly reduced to 54–90% compared with control cells transfected with NS miRNA oligos ($p < 0.05, 0.01$; miR-200a-5p: 0.92 ± 0.01, miR-532-3p: 0.54 ± 0.043, miR-680: 0.56 ± 0.008, miR-1901: 0.77 ± 0.018 vs. miR NS: 1). In contrast, luciferase activities in anti-miRNA oligo (inhibitor miRNA) transfected cells were significantly increased to 114 to 141% compared with control cells which were transfected with NS inhibitor miRNA ($p < 0.05, 0.01$; anti-miR-200a-5p: 1.14 ± 0.007, anti-miR-532-3p: 1.41 ± 0.023, anti-miR-680: 1.31 ± 0.12, anti-miR-1901: 1.13 ± 0.044 vs. anti-miR NS: 1). Note that mimic and inhibitors of miR-532-3p and miR-680 affected the luciferase activity more effectively than those of other miRNA, suggesting that miR-532-3p and miR-680 can exhibit more repressive activity at 3′UTR due to the presence of both canonical and non-canonical bindings.

Second, we evaluated if these miRNAs have repressive activity by binding at CDS, we co-transfected GFP tagged CDS of NMHC-IICmRNA with each of the mimic miRNAs in HEK293 cells, and checked the expression of NMHC-IIC-GFP using both immunoblots and fluorescence

Table 2. Base pairing of mRNA:miRNA at binding sites located at CDS and 3′UTR of NMHC-IIC mRNA (NM_001271538)

	CDS of NMHC-IIC mRNA		3′UTR of NMHC-IIC mRNA	
miRNA	Canonical site	Non-canonical site	Canonical site	Non-canonical site
200a-5p	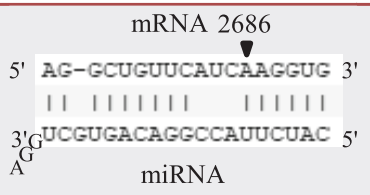		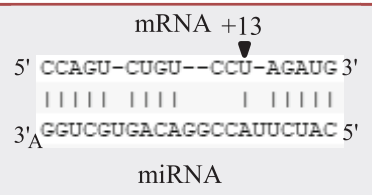	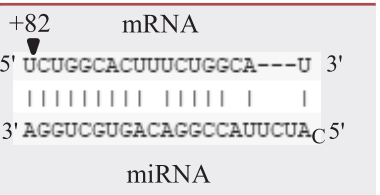
532-3p	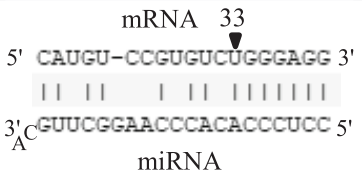	–		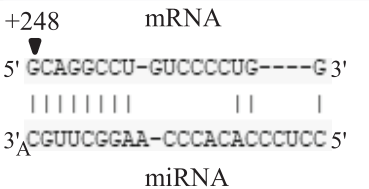
680	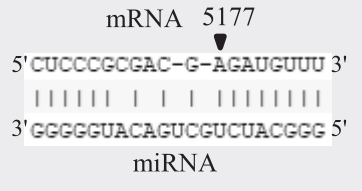	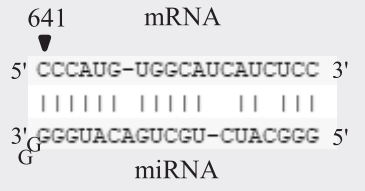		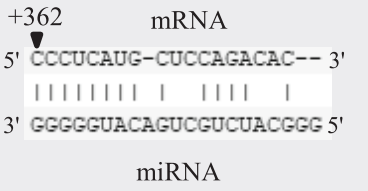
1901	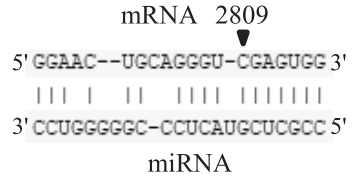		–	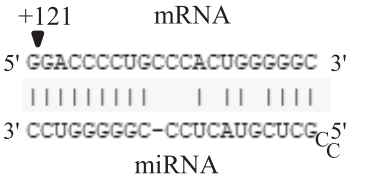

Base pairing is shown as per the miRepress at the binding sites (canonical or non-canonical). (+) indicates the positions relative to the stop codon and arrowheads indicate the starting nucleotides of the binding sites.

Figure 1. Network of miRNAs against NMHC-IIC mRNA

(A) The predicted miRNA-target network analysis by Cytoscape shows the other targets of the four miRNAs, apart from Myh14.

(B) Gene ontology biological process enrichment analysis of the predicted targets of four miRNAs—miR-200a-5p, miR-532-3p, miR-1901, and miR-680. The most enriched pathways are sorted according to their enrichment p value. Negative log 10 p value of enrichment is plotted along the x axis.

microscopy analyses (Figure S1). Expression of GFP-tagged NMHC-IIC was lower in the presence of each of the mimic miRNAs. Interestingly, the degree of repression of GFP reporters by individual mimic miRNA remained same as luciferase, suggesting that these miRNAs have almost similar site efficacy as 3′UTR (Figures 2B and S1A–S1D). Third, we assessed the repressive activity by checking the endogenous level of NMHC-IICmRNA (Figures 2D–2G) and protein (Figures 2H–2K) in each of the mimic miRNAs or inhibitors (anti-miRNA oligos) treated 4T1 cells. Figures 2D–2K show that the endogenous level of NMHC-IICmRNA and protein are maximally affected by miR-532-3p in 4T1 cells. We checked the effect of these miRNAs in other cells like MDA-MB 231, MCF-7 and Neuro-2a using luciferase assay (Figures S1E–S1G), where miR-532-3p showed the maximum site efficacy in target repression at both transcript stability and protein synthesis levels.

We checked the expression of miRNAs and NMHC-IIC in mouse lung and spleen tissues, if they can be correlated at the expression level. Like previous data,[35] we found an increased level of NMHC-IIC in the lung tissue compared with the spleen (Figure S2A). Interestingly, although the expression of miR-200a-5p, miR-680 and miR-1901 in spleen tissue was 1.2-fold increased, but miR-532-3p showed more than 2-fold in spleen compared with lung (Figures S2B and S2C). These data indicate that increase in expression of miRNA may correlate with the lower expression of NMHC-IIC in mouse spleen tissue, suggesting that the expression of NMHC-IIC can be regulated by miRNAs ensuing canonical and non-canonical binding.

Non-canonical binding represses the expression of NMIIC

To assess the effect of non-canonical (nc) binding at NMHC-IICmRNA by miRNA, which possess canonical (c) region, we perturbed the binding by incorporating point mutations at each of the binding sites located on 3′UTR of NMHC-IICmRNA, and looked for the luciferase activity in the presence of mimic miRNA in 4T1 cells. We considered the binding sites of miR-532-3p, which contains eight nucleotide length seed regions both at 5′end (c) and 3′ end (nc). Both the c and nc regions of miR-532-3p can complementarily pair with 3′UTR (+160 to +167) and (+247 to +254) sites, respectively. We replaced GG nucleotides with AA at + 162–163 (mutation at canonical site, MTc) or GC nucleotides with AA at +251–252 (mutation at non-canonical site, MTnc) of 3′UTR (Figure 3A). We co-transfected each of these MT 3′UTRs- or WT 3′UTR-luciferase with mimic miR-532-3p or NS miRNA (miR NS) to assess their repressive activity. We noticed that miR NS was not able to repress the luminescence signal in WT 3′UTR-luciferase expressing 4T1 cells. In contrast, the luminescence signal in WT 3′UTR-luciferase expressing 4T1 cells was 51 $\pm$ 3%, whereas that in MTc 3′UTR- and MTnc 3′UTR-luciferase expressing cells were 89 $\pm$ 2% and 69 $\pm$ 5% respectively, in the presence of mimic miR-532-3p suggesting that mutation at the canonical site has more blocking interference compared with non-canonical site in the expression of NMHC-IICmRNA (Figure 3B). We used a streptavidin-biotin pulldown strategy[36] to investigate the binding affinity of canonical and non-canonical regions with wildtype and mutants of 3′UTR of NMHC-IICmRNA. We co-transfected biotin-miR-532-3p with WT 3′UTR-, MTc 3′UTR- or MTnc 3′UTR tagged luciferase in 4T1 cells. The miRNA-mRNA complex was pulled down using streptavidin beads. Figures 3C and 3D shows that WT 3′UTR mRNA was 11.02 $\pm$ 1.29-fold enriched in the pellet of biotin-miR-532-3p compared with that of biotin-NS miRNA. In contrast, MTc 3′UTR- and MTnc 3′UTR mRNAs were only 3.1 $\pm$ 0.33 and 5.04 $\pm$ 0.54-fold enriched in the pellet, respectively, suggesting that mutation at the canonical site has more binding interference compared with non-canonical site in the miRNA:mRNA interaction. We also noticed that the amount of Argonaute 2 (AGO2) protein in the pellet was significantly reduced when the cells were transfected with MTnc 3′UTR (Figures 3E and 3F), thereby illustrating the formation of RNA-induced silencing complex at non-canonical site. Altogether these data suggest that effectiveness in binding of miR-532-3p correlates with the degree of inhibition in the expression of NMHC-IIC, and the presence of non-canonical site may play additive role in the miRNA mediated target repression.

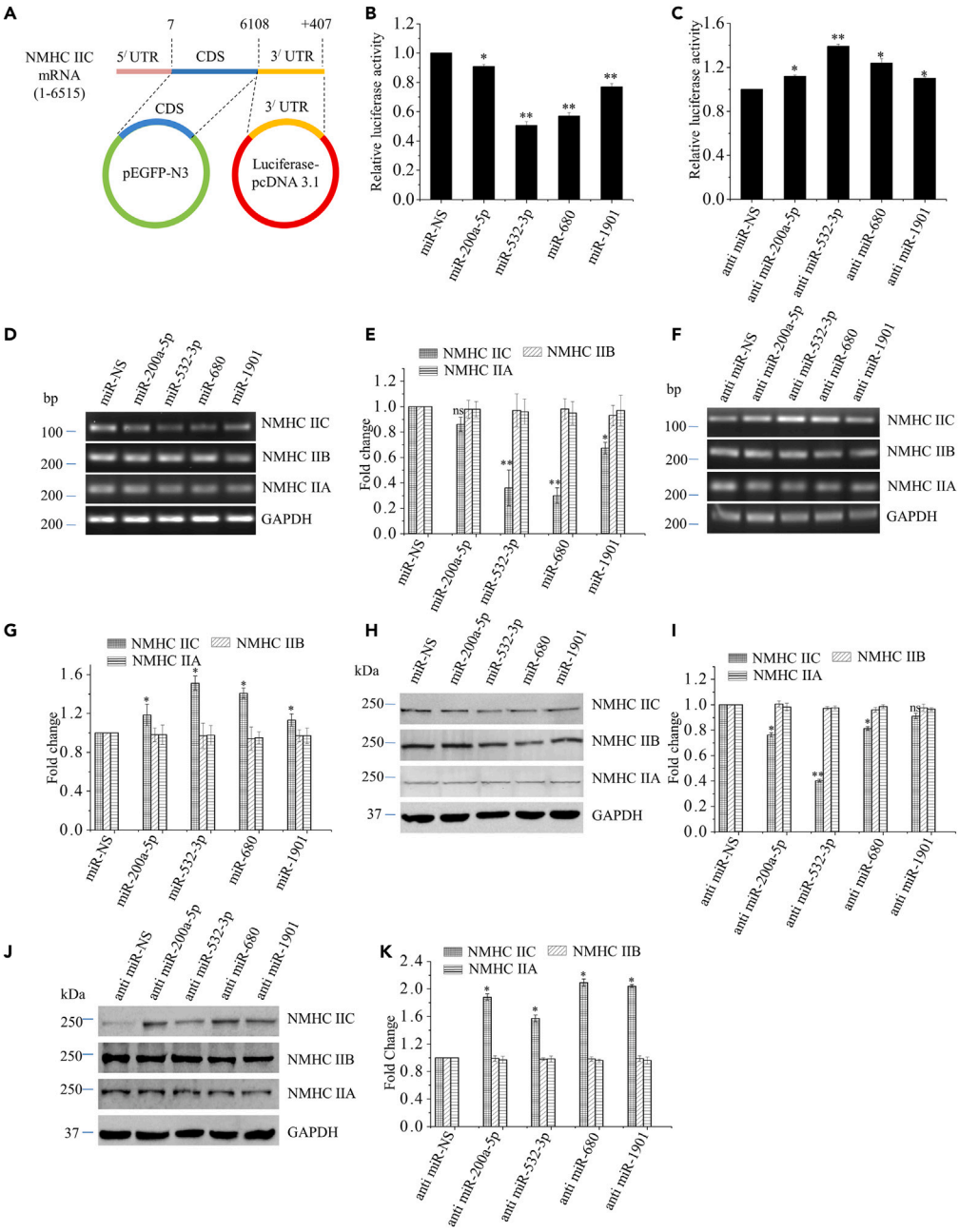

Figure 2. Canonical and non-canonical binding repress the expression of NMHC-IIC

(A) The schematic diagram shows the cloning of 3′UTR and CDS of NMHC-IIC mRNA in luciferase pcDNA 3.1 and pEGFP-N3 plasmid vectors, respectively.

(B and C) Dual luciferase assay of 4T1 cell lysates. The cells were co-transfected with a plasmid DNA encoding luciferase tagged 3′UTR and mimic miRNA (B) or inhibitor miRNA (anti-miRNA oligo) (C) against each of the four miRNAs. Fold change was calculated by considering the normalized luminescence signal from mimic NS miRNA (miR NS) (B) or inhibitor NS miRNA (anti-miR NS) (C) treated cell as "1."

(D–G) RT-PCR analysis of NMHC-IIs mRNA from each of the mimic miRNAs (D) or inhibitor miRNA (F) transfected 4T1 cells. Bands were visualized by EtBr staining. E and G show the quantification of band intensity of D and F, respectively.

(H–K) Immunoblot analysis of NMHC-IIs from 4T1 cells transfected with each of the mimic miRNAs (H) or inhibitor miRNAs (J) using antibodies, as indicated. I and K show the quantification of immunoblots shown in (H) and (J), respectively. Fold change was calculated by considering the relative band intensity of NMHC-IIs from miR NS or anti-miR NS treated cell as 1. GAPDH was used as a loading control. Data are presented as the mean ± SEM from three independent experiments. *$p < 0.05$, **$p < 0.01$; miR NS vs. mimic miRNA (B, E, and I) and anti-miR NS vs. anti-miRNA (C, G, and K). UTR, untranslated region; CDS, coding sequence.

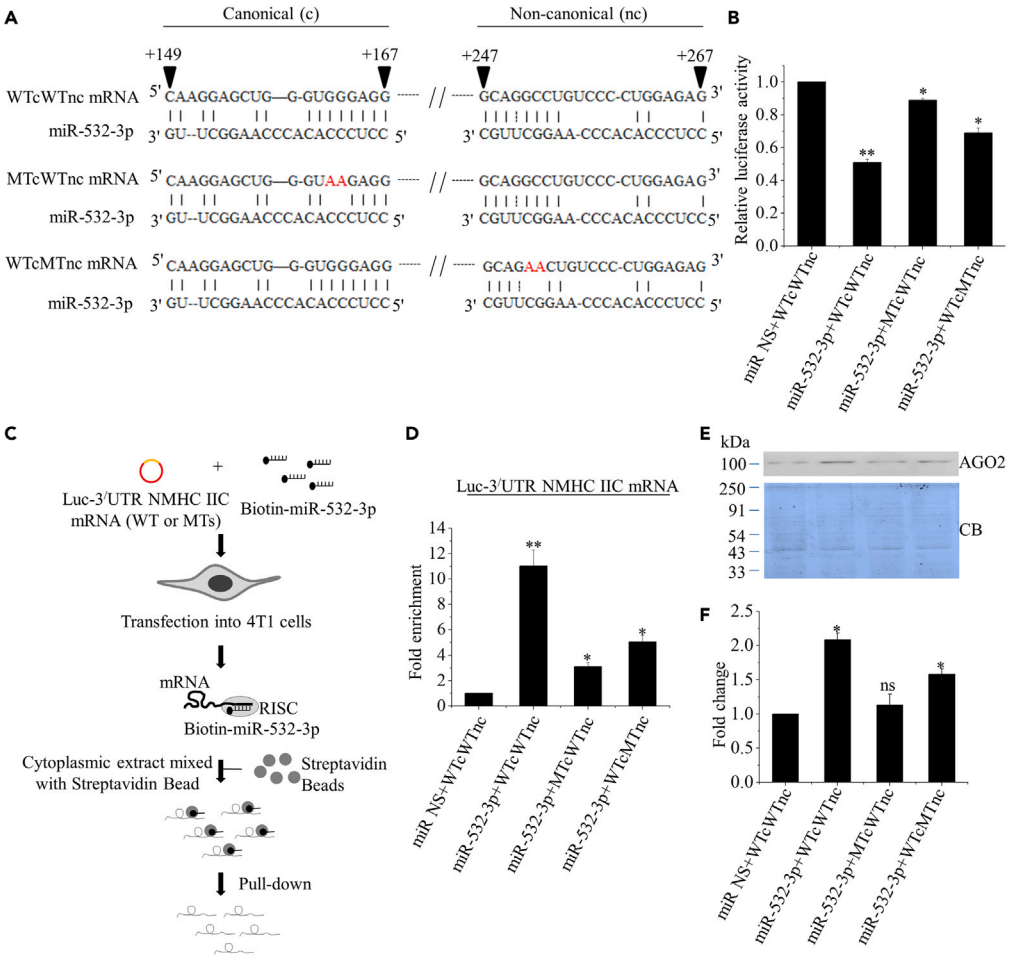

Figure 3. Loss of complementary base pairing at canonical and non-canonical regions decreases the binding ability of miR-532-3p with NMHC-IIC mRNA and AGO2

(A) The schematic diagram represents the canonical (c) binding site between 5′ end of miR-532-3p and 3′UTR (+149–167) and non-canonical (nc) site between 3′ end of miR-532-3p and 3′UTR (+247–267). The nucleotide number shown with black arrow-head at 3′UTR indicates the down-stream position from the stop codon. Red letters represent the mutated nucleotides at 3′UTR (MTc, MTnc).

(B) Dual luciferase assay using 4T1 cells co-transfected with mimic miR-532-3p and WT-, MTc-, or MTnc 3′UTR tagged luciferase. Fold change was calculated by considering the normalized luminescence signal from miR NS as "1."

(C) Schematic diagram of pulldown assay by biotin-conjugated mimic miR-532-3p.

(D) 4T1 cells were co-transfected with biotin-conjugated mimic miR-532-3p or miR NS, and luc- WT-, MTc- or MTnc 3′UTR of NMHC-IIC mRNA. The miRNA-mRNA complexes were pulled down by streptavidin beads. Enrichment of 3′UTR mRNAs was detected by qRT-PCR using primers specific to 3′UTR. Fold change was calculated by the $2^{-\Delta\Delta Ct}$ method. GAPDH was used as internal control. Data are represented as mean ± SEM from three independent experiments.

(E and F) Pellets in the pulldown assay were resolved on two SDS-PAGE in parallel. One was probed with antibody against AGO2, and other was stained with CB for loading control. (F) Quantification of immunoblot E. Fold change was calculated by considering the band intensity from miR NS and Luc-WT treated sample as "1." *$p < 0.05$, (miR NS + WT) vs. (miR-532-3p + MTc) or (miR-532-3p + MTnc); **$p < 0.01$, (miR NS + WT) vs. (miR-532-3p + WT). CB, Coomassie blue staining.

Altering the expression of NMHC-IIC increases both cellular migration and growth

Previous report established that inducible NMIIC functions as a mechanoresponsive element for tumor progression.[33] We were interested in checking if the major cellular processes in tumor progression such as migration or anchorage independent growth of 4T1 cells were affected by modulating the expression of NMHC-IIC by each of the four miRNAs. Firstly, we transfected each of these miRNA mimics or their inhibitors (anti-miRNA oligo), and looked for the cellular migration in both 2D and 3D setups. Figures S3A and S3B shows the time lapse images of 4T1 cells transfected with NS miRNA or mimic miRNAs (S3A and Video S1), and with NS or specific inhibitor (S3B and Video S2) for each of miRNA, respectively. We noticed that the cells transfected with mimic or inhibitor of miRNA possessed multiple filopodia like protrusions compared with control cells treated with mimic or inhibitor of NS miRNA (Figures S3C and S3D). Interestingly, cells transfected with miR-532-3p, miR-680, or miR-1901 mimic or inhibitor showed loss of front-rear asymmetry, relatively longer protrusion, and increased branching. Cells exhibited the fragmentation of branched protrusion or cell body (arrowheads, Figures S3A and S3B),

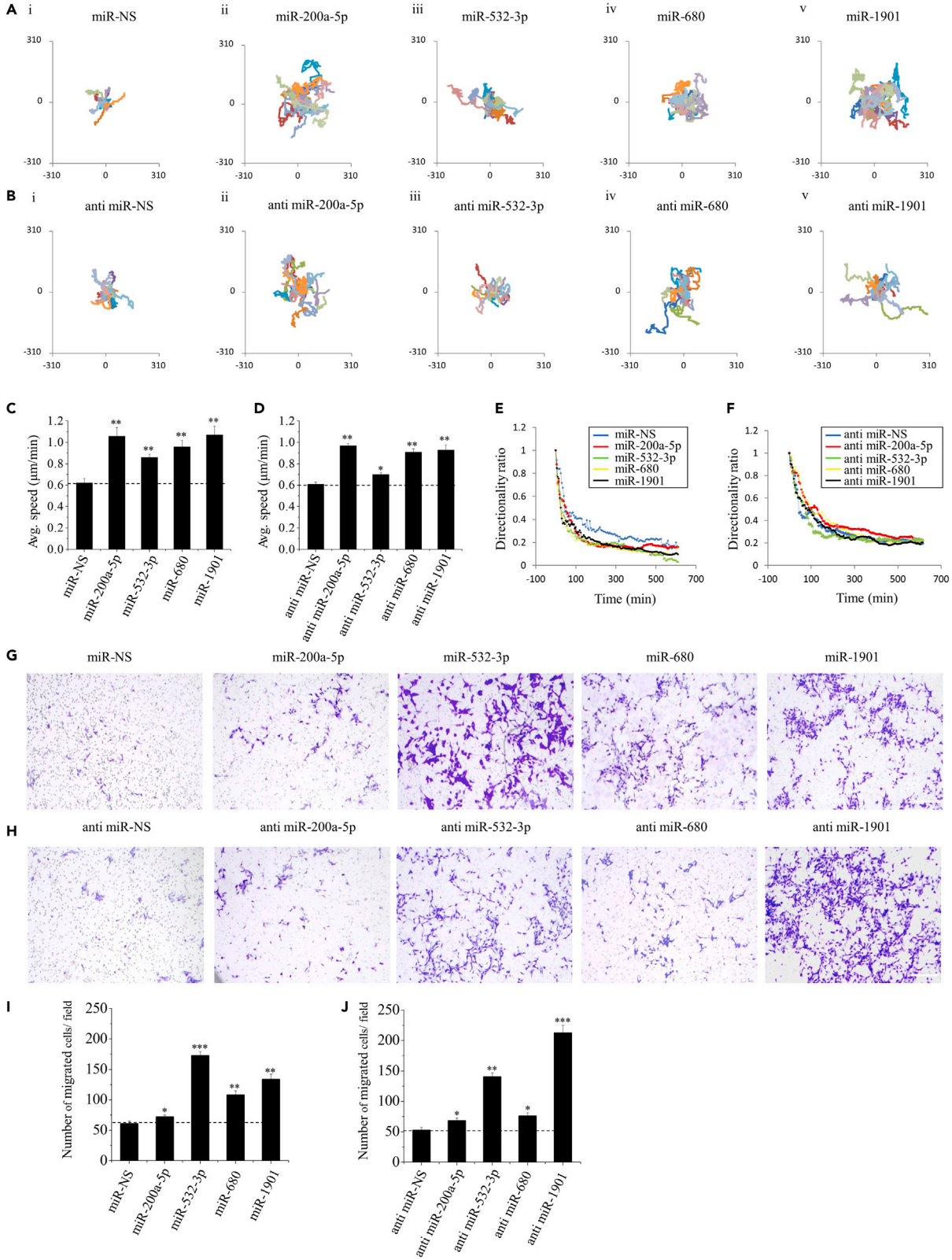
A
i
miR-NS
ii
miR-200a-5p
iii
miR-532-3p
iv
miR-680
v
miR-1901
B
i
anti miR-NS
ii
anti miR-200a-5p
iii
anti miR-532-3p
iv
anti miR-680
v
anti miR-1901
C
Avg. speed (μm/min)
miR-NS
miR-200a-5p
miR-532-3p
miR-680
miR-1901
D
Avg. speed (μm/min)
anti miR-NS
anti miR-200a-5p
anti miR-532-3p
anti miR-680
anti miR-1901
E
Directionality ratio
Time (min)
miR-NS
miR-200a-5p
miR-532-3p
miR-680
miR-1901
F
Directionality ratio
Time (min)
anti miR-NS
anti miR-200a-5p
anti miR-532-3p
anti miR-680
anti miR-1901
G
miR-NS
miR-200a-5p
miR-532-3p
miR-680
miR-1901
H
anti miR-NS
anti miR-200a-5p
anti miR-532-3p
anti miR-680
anti miR-1901
I
Number of migrated cells/ field
miR-NS
miR-200a-5p
miR-532-3p
miR-680
miR-1901
J
Number of migrated cells/ field
anti miR-NS
anti miR-200a-5p
anti miR-532-3p
anti miR-680
anti miR-1901

Figure 4. Mimic and inhibitor of the miRNAs increase cellular migration of 4T1 cells

(A and B) Cell trajectories were plotted for 4T1 cells transfected with each of the mimic miRNAs (Ai-v) or anti-miRNA oligos (Biv).

(C and D) Quantification of average speeds of mimic miRNA (C) or anti miRNA oligo (D) transfected 4T1 cells.

(E and F) Directionality ratios between the start and end of each cell trajectories of 4T1 cells transfected with mimic miRNA (E) or anti-miRNA oligo (F). Directional persistence of these migratory cells was quantified and analyzed from time lapse images of miRNA or anti miR oligo transfected 4T1 cells using DiPer program. n $\geq$ 10 cells from three independent experiments.

(G and H) *Trans* well migration: Representative bright-field images of migrated 4T1 cells transfected with mimic miRNA (G) or anti miRNA oligo (H).

(I and J) Quantification of migrated cells from (G) and (H), respectively. n $\geq$ 10 fields from three independent experiments. Data are represented as mean $\pm$ SEM. Scale bar: 100 μm. *p < 0.05, **p < 0.01; NS miR vs. mimic miRNAs and anti- NS miR vs. anti-miRNA.

which could be due to loss of coherent actomyosin contractility and the reduction of cortical tension. We found that each of mimic miRNA or their inhibitors increased migration and directionality compared with NS mimic or inhibitor miRNA (Figures 4A–4F). Interestingly, the mimic or inhibitor of miRNAs transfected cells showed increase in velocity such as miR-200a-5p transfected cells showed 70%, miR-532-3p 38%, miR-680 54% and miR-1901 72% compared with NS miR. On the other hand, inhibitor, anti-miR-200a-5p showed 57%, anti miR-532-3p: 14%, anti miR-680: 49%, and anti miR-1901: 52% increase in velocity compared with NS miRNA inhibitor (Figures 4C and 4D). Directionality ratios between the start and end of each cell trajectories were calculated as "1" for a straight cell trajectory and "close to 0" for a highly curved trajectory. Directional persistence and average speed of these migratory cells were quantified and analyzed from time lapse images using DiPer program (n $\geq$ 10 cells per sample) (Figures 4E and 4F). We also checked the effect of miRNA in collective cell migration using time lapse microscopy. At 12 h, miR-532-3p and miR-1901 transfected cells in collective mode showed significantly increased migration and hence decreased wound area in comparison with NS miR mimic or inhibitor transfected cells (decrease of wound area, miR-200a-5p: 2%, miR-532-3p:13%, miR-680: 9%, miR-1901: 17% and anti miR-200a-5p: 3.5%, anti miR-532-3p: 8%, anti miR-680: 7%, anti miR-1901: 12%, Figures S4A–S4D). Similarly, miR-532-3p and miR-1901 showed increase in the number of migrated cells (miR-200a-5p: 16%, miR-532-3p:175%, miR-680: 72%, miR-1901: 108% and inhibitor, anti miR-200a-5p: 26%, anti miR-532-3p: 173%, anti miR-680: 36%, anti miR-1901: 298%) under 3D setup (Figures 4G–4J).

Secondly, we carried out soft agar colony assay to investigate cellular growth with 4T1 cells transfected with mimic or anti-miRNA oligos. Interestingly, both mimic miRNA and their inhibitor transfected cells showed an increase in colony area (n $\geq$ 50) and colony number compared with control cells transfected with NS miRNA mimic and inhibitor, respectively (miR-200a-5p: 23%, miR-532-3p: 31%, miR-680: 24%, miR-1901: 43% increase compared with miR NS, and anti miR-200a-5p: 20%, anti miR-532-3p: 27%, anti miR-680: 23%, anti miR-1901: 32% increase compared with NS miRNA inhibitor at day 14, Figures 5A–5C). Taking together these data suggest that changing the expression level of NMIIC by any of these four miRNAs increases cellular migration and growth.

Threshold amount of NMIIC is associated with tumorigenic ability of 4T1 cells

In order to examine whether up and down expression of NMIIC can affect growth of tumor cells *in vivo*, we subcutaneously injected 4T1 cells, which were previously transfected with mimic miRNA or anti miRNA oligos, in mice. Figures 5D and S5 show representative images of tumor tissues developed in mice at 32 days post injection (dpi) and H&E staining of the corresponding tumor tissue sections, respectively. H&E staining indicates the presence of tumorigenic cells at the site of injection. Note that a significant increase in tumor size was observed in the presence of each of four miRNAs mimic or their inhibitors compared with nonspecific mimic or inhibitor, respectively. Increase in tumor size was correlated with increase in cell proliferation as evident from proliferation cell nuclear antigen (PCNA) staining of the section next to H&E staining (Figures 5D–5G). We checked the level of MYH14, miR-532-3p and miR-200a-5p in various types of human cancers in GEPIA and dbDEMC database, which provided the expression profiles of genes in different cancers. In few instances, the expression level of MYH14 was inversely correlated with hsa-miR-532-3p in COAD, HNSC, KIRC, MESO, OV, THCA, and UCS whereas with hsa-miR-200a-5p in ACC, COAD, LIHC, and ESCA (Figures S6A and S6B). With our available tumor sample analysis, we found that the level of NMHC-IICmRNA was 1.47 $\pm$ 0.34 and 1.53 $\pm$ 0.37-fold increase in gastric cancer and contralateral sarcoma, respectively whereas that was 0.73 $\pm$ 0.27-fold in colon cancer compared with normal tissue associated with tumor (NTAT) tissues (Figure S6C). Interestingly, we found hsa-miR-532-3p was 2.36 $\pm$ 0.25-fold up regulated in colon cancer and 2.99 $\pm$ 0.65-fold in gastric cancer, but down regulated in contralateral sarcoma (0.81 $\pm$ 0.55-fold). In contrast, hsa-miR-200a-5p was 2.11 $\pm$ 0.65-fold up regulated in gastric cancer and 2.02 $\pm$ 0.67-fold in contralateral sarcoma but 0.66 $\pm$ 0.35-fold down regulated in colon cancer. Altogether, these data suggest that threshold amount of NMIIC may be maintained to prevent from tumorigenesis, and the transcript of NMHC-IIC is regulated by more than one miRNA.

Affecting NMIIC expression changes the fraction of heterofilament formation

Previously, Surcel et al.[33] established that increase or decrease of NMIIC level significantly reduced the cortical tension in cancer cells. The cancer cells with reduced cortical tension become more mechanoresponsive such that they can survive and grow in different variety of extracellular matrix.[33] The abundance of individual paralogs of NMII and their ability to form heterofilament may contribute to the overall cortical tension of the cell. As the expression of paralog IIA and IIB remained unaltered in the presence of miRNAs mimic or inhibitor, we were prompted to investigate whether the amount of NMHC-IIC affects the hetero-filament formation with other paralogs NMHC-IIA and -IIB in the cells. In order to detect endogenous interactions with NMHC-IIA and -IIB, we immunoprecipitated NMIIA and -IIB, and looked for NMIIC in the immunoprecipitates. In presence of mimic miR-532-3p, the fractions of NMIIA-IIC and NMIIB-IIC heterotypic

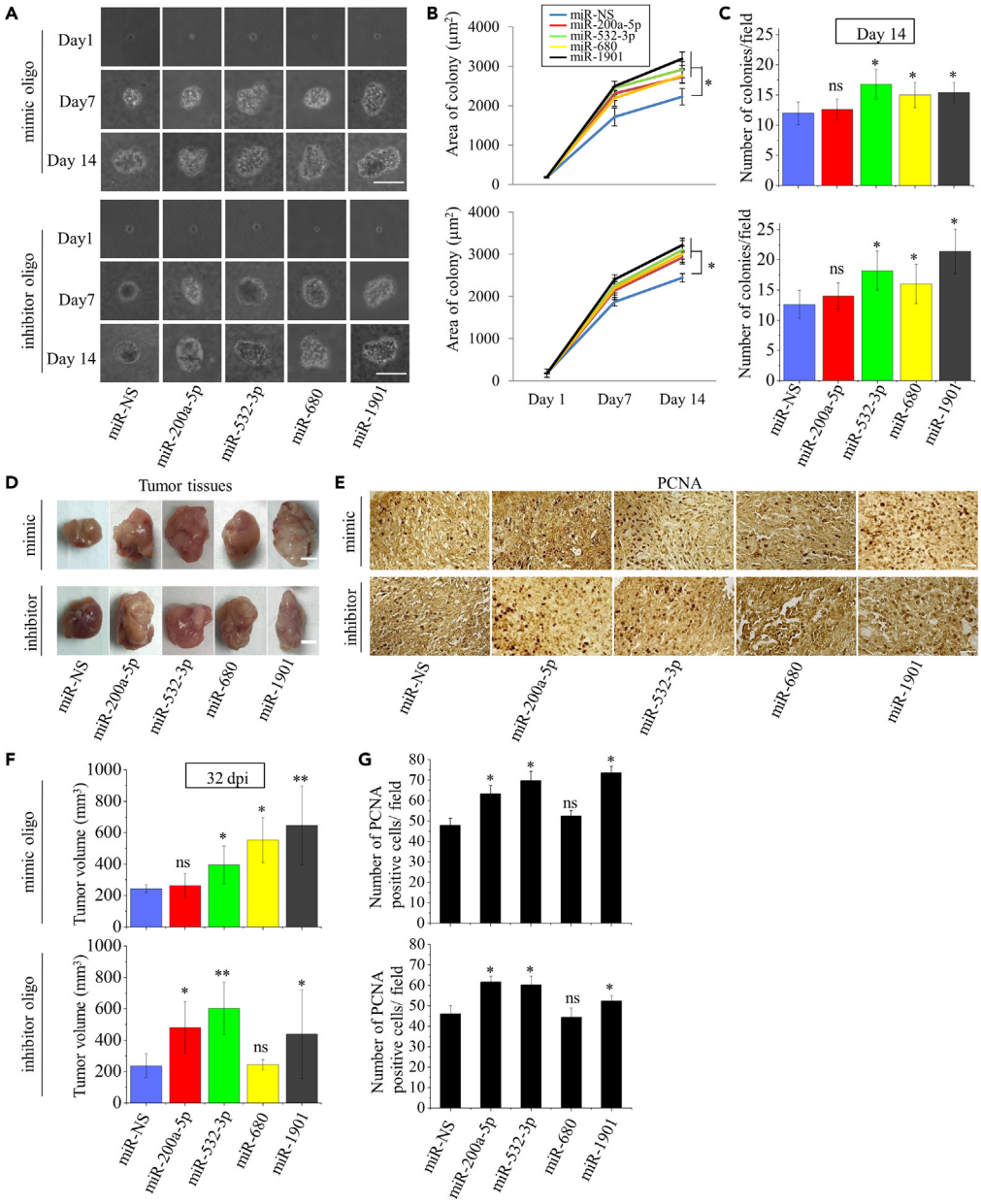

Figure 5. Mimic and inhibitor of the miRNAs increase tumorigenic ability of 4T1 cells

(A) Representative bright field images of soft agar colonies of 4T1 cells transfected with mimic miRNAs or anti-miRNA oligos.

(B and C) Quantification of colony area (B) and number of colonies (C). $n \geq 50$ colonies from three independent experiments.

(D and E) Representative images of tumor tissues at 32 dpi and their PCNA staining. Mice were injected with 4T1 cells which were previously transfected with mimic or anti-miRNA oligos.

(F and G) Quantification of tumor size at 32 dpi (F), and the number of PCNA positive cells per field (G). Data are represented as mean ± SEM. n ≥ 9 fields of three tumors (n = 3 mice). *p < 0.05, **p < 0.01; miR-NS vs. mimic or anti-miR-NS vs. anti-miR. dpi, days post injection. Scale bar: 50 μm (A), 5 mm (D), and 100 μm (E).

filaments were decreased whereas inhibitor of miR-532-3p increased the heterofilaments formation despite the no change in the expression of NMIIA and -IIB in mimic or inhibitor transfected cells (Figures 6A–6D). Similarly, we checked heterofilament formation in cells co-expressing NMHC-IIC-GFP and NMHC-IIA-mCherry, or NMHC-IIC-GFP and NMHC-IIB-mCherry. Figures 6E and 6F show the heterofilaments formation (arrowhead and appearance of fluctuation of each fluorescence intensity across the line) in the presence of miR-532-3p inhibitor. Interestingly, cytoskeleton fraction of NMIIC remained unchanged whereas that of NMIIA and IIB was decreased in mimic or inhibitor transfected cells (Figures 6G and 6H). Altogether, these data suggest that the amount of NMIIC controls the cytoskeletal fraction of NMIIA and NMIIB.

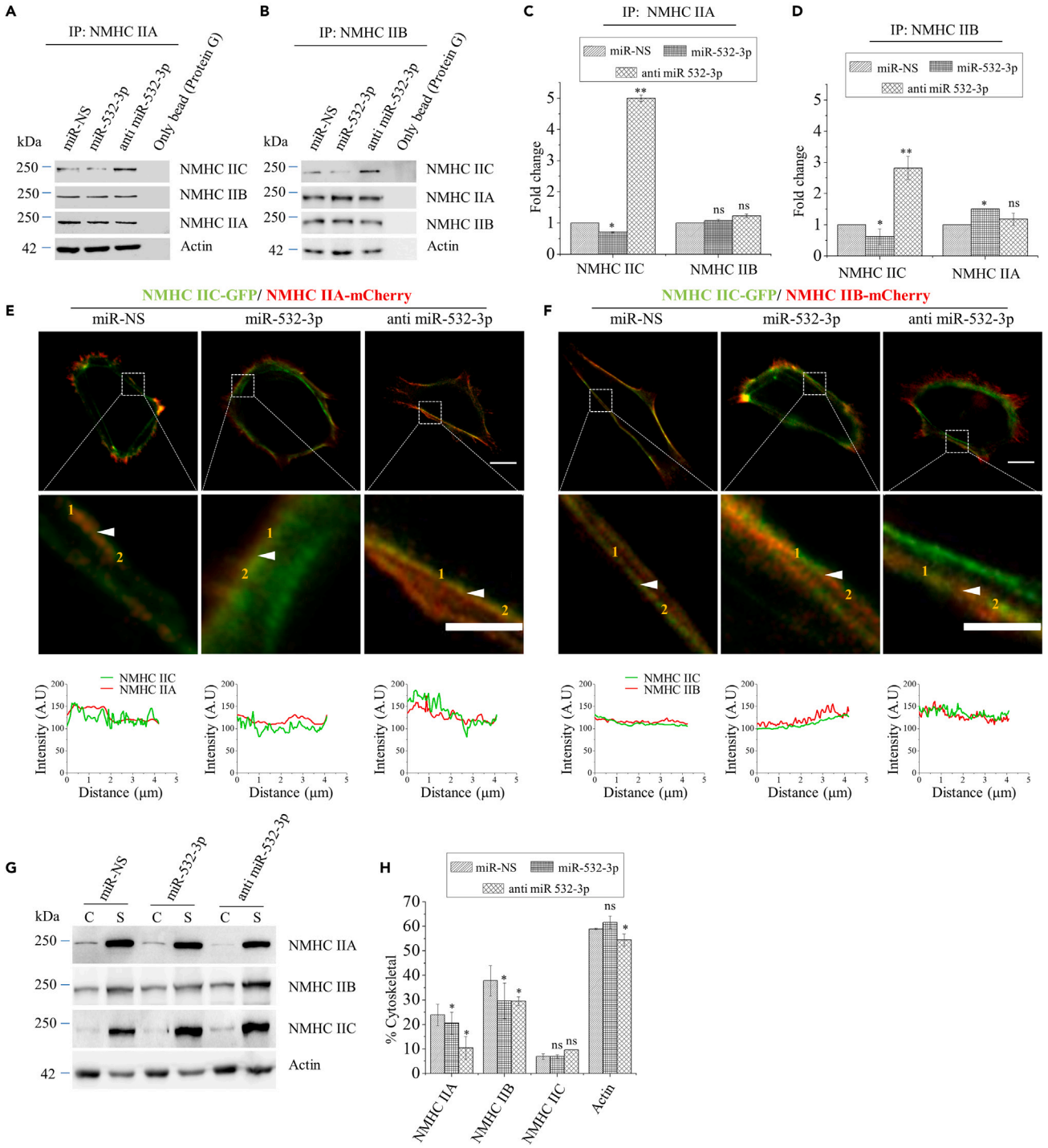

Figure 6. NMHC-IIC forms heterotypic filaments with other paralogs

(A and B) Cell lysates from mimic miR-532-3p or anti-miR-532-3p transfected 4T1 cells were subjected to immunoprecipitation (IP) with anti-NMHC-IIA (A) or anti-NMHC-IIB (B) antibody followed by immunoblot analyses with NMHC-IIA, -IIB, -IIC or actin antibody. Only bead (protein G) was taken as a control for IP. Immunoblot with NMHC-IIA and NMHC-IIB antibodies were used as input controls for A and B, respectively.

(C and D) Quantification of immunoblots of A and B.

(E and F) Confocal microscopy of 4T1 cells co-transfected with nonspecific miR, mimic miR-532-3p, or anti-miR-532-3p, and NMHC-IIC-GFP, and NMHC-IIA-mCherry (E) or NMHC-IIB- mCherry (F). The dashed rectangles indicated in the panels are magnified and shown below. Arrowheads denote heterofilaments.

Figure 6. *Continued*

Line profiles of fluorescence intensity (AU) of NMHC-IIC-GFP and NMHC-IIA-mCherry or NMHC-IIB-mCherry were obtained from the line between point 1 and 2 in the magnified images. n > 8 cells from three independent experiments. Scale bar: 10 μm and 5 μm (magnified image).

(G) Cytoskeletal fraction of NMII in the presence of mimic miR-532-3p or its inhibitor. Triton X-100 soluble and insoluble fractions were probed with NMHC-IIA, -IIB, -IIC or actin antibody.

(H) Quantification of immunoblot. (%) of cytoskeletal fraction was calculated by considering the following equation; (%) = [band intensity cytoskeletal (C)/ cytoskeletal (C) + soluble (S)] *100. Data are represented as mean ± SEM from three independent experiments. *p < 0.05, **p < 0.01; miR NS vs. mimic miR-532-3p and anti-miR NS vs. anti-miR-532-3p.

DISCUSSION

MiRNAs provide an extra layer of complexity in the context of gene regulation. In this report, we provide evidences that the expression of NMIIC, a low abundant mechanoresponsive protein which has previously been shown to be involved in maintaining cortical tension in cancer cells, can be regulated by miRNAs through both canonical and non-canonical binding.

Recent studies established the expression of NMIIA and -IIB can be regulated by miRNA let-7f and hsa-miR-181a-5p, respectively.[27,28] Our study on the expression of NMIIC strengthens an idea that NMII paralogs are regulated by miRNAs. The involvement of multiple miRNAs may provide more complexity in the regulation of NMIIC as each of the miRNAs differs in terms of functional importance, and possesses both canonical and non-canonical binding regions. There are non-canonical miRNAs which are classified based on their biogenesis. Generally, they bypass one or more steps of the classic canonical biogenesis pathway.[37,38] These non-canonical miRNAs are found to be originated from introns, snoRNAs, endogenous shRNAs and tRNAs. However, in this article, we demonstrate non-canonical miRNA based on complementary base pairing at 3′end of miRNA, which can also repress the target gene expression similar to previous report.[39] We find miR-1901, encoded by a novel lnc-RNA generated from the anti-sense strand of Cables gene,[40] has two non-canonical and one canonical binding sites at NMHC-IIC mRNA (Table 2), out of which only one non-canonical site is present at 3′UTR. Here, we provide evidence that miR-1901 can repress 3′UTR of NMHC-IIC-luciferase mRNA significantly despite having no canonical binding site at 3′UTR (Figure 2B), suggesting that non-canonical binding plays significant role in mRNA:miRNA interaction to inhibit the gene expression. Although previous reports have described the non-significant effect by non-canonical binding,[4] we find rather significant reduction in gene expression (Figure 3), further highlighting the importance of non-canonical binding.[41,42]

We notice that the degree of effectiveness in repressing NMIIC expression or affecting cellular function significantly varies among the four miRNAs—miR-200a-5p, miR-532-3p, miR-680, and miR-1901—despite their ability to bind both at 3′UTR and CDS canonically as well as non-canonically (Figures 2 and S1), suggesting the possibility of other factors which can determine the efficacy of miRNA binding with mRNA and consequently its repressive activity. We summarize those multiple factors as follows. (1) Proximity of binding site—miR-680 has two binding sites, but their close proximity may effectively allow to use one of the two sites,[43] which can be attributed to less effectiveness in repressing 3′UTR of NMHC-IIC mRNA. (2) Presence of wobble base pairing and access to silencing complex-miR-532-3p has more effective repressive ability among the four miRNAs. Note that miR-532-3p exhibit a 7mer-m8 seed as well as a 6mer seed base pairing at 3′UTR and CDS of NMHC-IIC mRNA, respectively. We also notice that miR-532-3p possesses significantly less number of G:U wobble base pairing compared with other three miRNAs (Table 2). (3) Abundance of miRNA—the amount of intracellular miRNA can be affected by the presence of extracellular vesicle loaded with miRNAs.[44] We find the presence of all the four miRNAs in the shed microvesicles (50–1500 nm in size) (Figures S6D and S6E). Interestingly, GEO dataset also reveals the presence of miR-532-3p and miR-1901 in 4T1exosome (Figure S6F).

Previous study suggests that overexpression and knockdown of NMIIC has a profound impact on cell mechanic, leading to an overall reduction in cortical tension of 20% and 40%, respectively in pancreatic cancer cells.[33] NMIIC has a similar impact on mechanic in colorectal cancer cells, where it also constitutes a small percentage of the total myosin II.[45] Our finding with siRNA-based NMIIC knockdown cells further supports the idea that changing the expression of NMIIC leads to increase in cancer cell migration (Figures 4, S3, S4, and S7). But how is increase or decrease of NMIIC expression linked with reduction of cortical tension? As the expression of NMIIA and IIB remained unchanged in miRNA mimic or inhibitor treated cells, their co-assembly with NMIIC may play significant role in maintaining cortical tension. Unlike NMIIA or -IIB, NMIIC minifilaments contain ~14 molecules, consist of a longer bare zone, and differ in terms of the charge distribution in their nonhelical tails. These features lead to a low fraction of molecules, which are stably bound together with the other isoforms, i.e., NMIIA and NMIIB.[46,47] Heterotypic minifilament formation could be mechanosensor of the contractile actomyosin unit to provide fine-tuning of mechanoresponse as the ratio of active NMIIA and NMIIB determines the transition of heterotypic NMIIA/B minifilaments from slip to catch-bond like behaviors.[13,48] We hypothesize the dual role of NMIIC. When the expression of NMIIC is below the threshold amount, fraction of NMIIC minifilament with actin filament is less (rate of inclusion of NMIIC monomer into filament may be less) and hence less cortical tension. In contrast, if the expression of NMIIC is above the threshold amount, fraction of NMIIC minifilament may remain same as NMIIC monomer are loosely bound to each other and hence less stable, rather fraction of NMIIB/C and NMIIA/C will be high and hence fraction of only NMIIA and -IIB minifilaments may be less in cytoskeleton fraction (as total amount of each isoform remain unchanged). So, beyond the threshold amount NMIIC, cortical tension is reduced due to the change in fraction of each type of homo and heterofilaments associated with the actin filament (Figures 6 and S8). Smith et al.[49] have established that decrease in the number of NMIIA filaments associated with local and nanoscale membrane oscillations, suggesting decreased membrane tension in red blood cells. Thus, decline in the cytoskeletal NMII fraction might also cause the reduction in the cortical tension. The external factor like external force has already been established to induce the association of myosin filament with actin, here we provide evidence for the first time that an internal factor like low abundance of an isoform, which can influence the fraction of homotypic or heterotypic filaments of others, and hence cortical tension. Our report describing non-canonical binding beyond

3′UTR and seed regions, make the rules governing miRNA mediated gene regulation even more complex. The concept of "on-target" (specific) and "off-target" (nonspecific) interactions may be an oversimplification when it is applied to physiologic regulation, as miRNA mediated gene regulation may be the outcome of many types of interactions between miRNAs and target mRNAs. Our study suggests that both "primary" target sites (canonical) where high affinity interactions take place and "secondary" lower affinity sites (non-canonical), are involved in regulating the gene expression effectively in physiological or pathophysiological conditions, and opens a window for designing therapeutic approach against miRNA-based therapy.

Limitations of the study

Although we have found evidence that miR-532-3p may regulate NMHC-IIC by binding to both canonical and non-canonical sites in the 3′UTR of NMIIC's HC mRNA, there are some limitations to our study that must be acknowledged. We have not checked the importance of non-canonical interactions at the CDS of NMHC-IIC mRNA and the existence of canonical and non-canonical miRNA based regulation of NMIIC in normal cells. Additionally, the number of cancer patients included in our study was limited, which may affect the generalizability of our conclusions.

STAR★METHODS

Detailed methods are provided in the online version of this paper and include the following:

- KEY RESOURCES TABLE
- RESOURCE AVAILABILITY
  - Lead contact
  - Materials availability
  - Data and code availability
- EXPERIMENTAL MODEL AND STUDY PARTICIPANT DETAILS
  - Cell lines
  - Laboratory animals
- METHOD DETAILS
  - miRNA and plasmid DNA transfection
  - SiRNA transfection
  - Bioinformatics analysis
  - Dual luciferase assay
  - Immunoprecipitation, immunoblot and SDS-PAGE
  - RNA isolation, cDNA preparation and qRTPCR
  - Biotin-miR-532-3p pulldown assay
  - Soft agar colony assay
  - Cell migration and live cell imaging
  - Cytoskeletal fractionation
  - *In vivo* tumor formation in mice and immunohistochemistry
  - Cloning of 3/UTR and CDS of NMHC-II mRNA
  - Immunofluorescence confocal microscopy
  - Would healing assay
  - Extracellular vesicle isolation
  - Total RNA isolation from human tissues, cDNA preparation and qRTPCR
- QUANTIFICATION AND STATISTICAL ANALYSIS

SUPPLEMENTAL INFORMATION

Supplemental information can be found online at https://doi.org/10.1016/j.isci.2023.108384.

ACKNOWLEDGMENTS

We thank Dr. Surajit Sinha, IACS for technical help for carrying out experiment with luminometer. We also thank DST-INSPIRE and CSIR for fellowship to K.B. and I.G., respectively. We thank TRC project, Department of Science and Technology, Government of India (AI/1/62/IACS/2015(C), and IACS for financial support.

AUTHOR CONTRIBUTIONS

S.S.J. conceptualized the study. K.B., S.S., and I.G. performed experimental work. S.G., S.D., and K.B. carried out bioinformatics analysis. K.B. and S.S.J. contributed to analyze the results and prepare the figures. K.B. wrote the initial draft of the manuscript. S.S.J. edited the manuscript with input from all the authors.

DECLARATION OF INTERESTS

The authors declare no competing or financial interests.

Received: May 17, 2023
Revised: September 27, 2023
Accepted: October 30, 2023
Published: November 2, 2023

REFERENCES

1. Lewis, B.P., Burge, C.B., and Bartel, D.P. (2005). Conserved seed pairing, often flanked by adenosines, indicates that thousands of human genes are microRNA targets. Cell *120*, 15–20. https://doi.org/10.1016/j.cell.2004.12.035.
2. Lewis, B.P., Shih, I.H., Jones-Rhoades, M.W., Bartel, D.P., and Burge, C.B. (2003). Prediction of mammalian microRNA targets. Cell *115*, 787–798. https://doi.org/10.1016/s0092-8674(03)01018-3.
3. Chi, S.W., Hannon, G.J., and Darnell, R.B. (2012). An alternative mode of microRNA target recognition. Nat. Struct. Mol. Biol. *19*, 321–327. https://doi.org/10.1038/nsmb.2230.
4. Agarwal, V., Bell, G.W., Nam, J.W., and Bartel, D.P. (2015). Predicting effective microRNA target sites in mammalian mRNAs. Elife *4*, 05005. https://doi.org/10.7554/eLife.05005.
5. Hausser, J., Syed, A.P., Bilen, B., and Zavolan, M. (2013). Analysis of CDS-located miRNA target sites suggests that they can effectively inhibit translation. Genome Res. *23*, 604–615. https://doi.org/10.1101/gr.139758.112.
6. Karginov, F.V., and Hannon, G.J. (2013). Remodeling of Ago2–mRNA interactions upon cellular stress reflects miRNA complementarity and correlates with altered translation rates. Genes Dev. *27*, 1624–1632. https://doi.org/10.1101/gad.215939.113.
7. Wynendaele, J., Böhnke, A., Leucci, E., Nielsen, S.J., Lambertz, I., Hammer, S., Sbrzesny, N., Kubitza, D., Wolf, A., Gradhand, E., et al. (2010). An illegitimate microRNA target site within the 3′ UTR of MDM4 affects ovarian cancer progression and chemosensitivity. Cancer Res. *70*, 9641–9649. https://doi.org/10.1158/0008-5472.CAN-10-0527.
8. Lujambio, A., Calin, G.A., Villanueva, A., Ropero, S., Sánchez-Céspedes, M., Blanco, D., Montuenga, L.M., Rossi, S., Nicoloso, M.S., Faller, W.J., et al. (2008). A microRNA DNA methylation signature for human cancer metastasis. Proc. Natl. Acad. Sci. USA *105*, 13556–13561. https://doi.org/10.1073/pnas.0803055105.
9. Scott, G.K., Mattie, M.D., Berger, C.E., Benz, S.C., and Benz, C.C. (2006). Rapid alteration of microRNA levels by histone deacetylase inhibition. Cancer Res. *66*, 1277–1281. https://doi.org/10.1158/0008-5472.CAN-05-3632.
10. Peng, Y., and Croce, C.M. (2016). The role of MicroRNAs in human cancer. Signal Transduct. Target. Ther. *1*, 15004–15009. https://doi.org/10.1038/sigtrans.2015.4.
11. Vicente-Manzanares, M., Zareno, J., Whitmore, L., Choi, C.K., and Horwitz, A.F. (2007). Regulation of protrusion, adhesion dynamics, and polarity by myosins IIA and IIB in migrating cells. J. Cell Biol. *176*, 573–580. https://doi.org/10.1083/jcb.200612043.
12. Vicente-Manzanares, M., Koach, M.A., Whitmore, L., Lamers, M.L., and Horwitz, A.F. (2008). Segregation and activation of myosin IIB creates a rear in migrating cells. J. Cell Biol. *183*, 543–554. https://doi.org/10.1083/jcb.200806030.
13. Vicente-Manzanares, M., Ma, X., Adelstein, R.S., and Horwitz, A.R. (2009). Non-muscle myosin II takes centre stage in cell adhesion and migration. Nat. Rev. Mol. Cell Biol. *10*, 778–790. https://doi.org/10.1038/nrm2786.
14. Aguilar-Cuenca, R., Juanes-García, A., and Vicente-Manzanares, M. (2014). Myosin II in mechanotransduction: master and commander of cell migration, morphogenesis, and cancer. Cell. Mol. Life Sci. *71*, 479–492. https://doi.org/10.1007/s00018-013-1439-5.
15. Komatsu, S., and Ikebe, M. (2007). The phosphorylation of myosin II at the Ser1 and Ser2 is critical for normal platelet-derived growth factor induced reorganization of myosin filaments. Mol. Biol. Cell *18*, 5081–5090. https://doi.org/10.1091/mbc.e06-12-1076.
16. Abedrabbo, M., and Ravid, S. (2020). Scribble, Lgl1, and myosin II form a complex *in vivo* to promote directed cell migration. Mol. Biol. Cell *31*, 2234–2248. https://doi.org/10.1091/mbc.E19-11-0657.
17. Clark, K., Middelbeek, J., Lasonder, E., Dulyaninova, N.G., Morrice, N.A., Ryazanov, A.G., Bresnick, A.R., Figdor, C.G., and van Leeuwen, F.N. (2008). TRPM7 regulates myosin IIA filament stability and protein localization by heavy chain phosphorylation. J. Mol. Biol. *378*, 790–803. https://doi.org/10.1016/j.jmb.2008.02.057.
18. Dulyaninova, N.G., Malashkevich, V.N., Almo, S.C., and Bresnick, A.R. (2005). Regulation of myosin-IIA assembly and Mts1 binding by heavy chain phosphorylation. Biochem *44*, 6867–6876. https://doi.org/10.1021/bi0500776.
19. Zhai, K.F., Zheng, J.R., Tang, Y.M., Li, F., Lv, Y.N., Zhang, Y.Y., Gao, Z., Qi, J., Yu, B.Y., and Kou, J.P. (2017). The saponin D39 blocks dissociation of non-muscular myosin heavy chain IIA from TNF receptor 2, suppressing tissue factor expression and venous thrombosis. Br. J. Pharmacol. *174*, 2818–2831. https://doi.org/10.1111/bph.13885.
20. Zhai, K., Duan, H., Wang, W., Zhao, S., Khan, G.J., Wang, M., Zhang, Y., Thakur, K., Fang, X., Wu, C., et al. (2021). Ginsenoside Rg1 ameliorates blood–brain barrier disruption and traumatic brain injury via attenuating macrophages derived exosomes miR-21 release. Acta Pharm. Sin. B *11*, 3493–3507. https://doi.org/10.1016/j.apsb.2021.03.032.
21. Weber, M., Kim, S., Patterson, N., Rooney, K., and Searles, C.D. (2014). MiRNA-155 targets myosin light chain kinase and modulates actin cytoskeleton organization in endothelial cells. Am. J. Physiol. Heart Circ. Physiol. *306*, 1192–1203. https://doi.org/10.1152/ajpheart.00521.2013.
22. Adyshev, D.M., Moldobaeva, N., Mapes, B., Elangovan, V., and Garcia, J.G.N. (2013). MicroRNA regulation of nonmuscle myosin light chain kinase expression in human lung endothelium. Am. J. Respir. Cell Mol. Biol. *49*, 58–66. https://doi.org/10.1165/rcmb.2012-0397OC.
23. Landais, S., Landry, S., Legault, P., and Rassart, E. (2007). Oncogenic potential of the miR-106-363 cluster and its implication in human T-cell leukemia. Cancer Res. *67*, 5699–5707. https://doi.org/10.1158/0008-5472.CAN-05-3632.
24. Pellegrino, L., Stebbing, J., Braga, V.M., Frampton, A.E., Jacob, J., Buluwela, L., Jiao, L.R., Periyasamy, M., Madsen, C.D., Caley, M.P., et al. (2013). miR-23b regulates cytoskeletal remodeling, motility and metastasis by directly targeting multiple transcripts. Nucleic Acids Res. *41*, 5400–5412. https://doi.org/10.1093/nar/gkt245.
25. Jurmeister, S., Baumann, M., Balwierz, A., Keklikoglou, I., Ward, A., Uhlmann, S., Zhang, J.D., Wiemann, S., and Sahin, Ö. (2012). MicroRNA-200c represses migration and invasion of breast cancer cells by targeting actin-regulatory proteins FHOD1 and PPM1F. Mol. Cell Biol. *32*, 633–651. https://doi.org/10.1128/MCB.06212-11.
26. Liang, S., He, L., Zhao, X., Miao, Y., Gu, Y., Guo, C., Xue, Z., Dou, W., Hu, F., Wu, K., et al. (2011). MicroRNA let-7f inhibits tumor invasion and metastasis by targeting MYH9 in human gastric cancer. PLoS One *6*, 18409. https://doi.org/10.1371/journal.pone.0018409.
27. Song, M., Li, Y., Chen, Z., Zhang, J., Yang, L., Zhang, F., Song, C., Miao, M., Chang, W., and Shi, H. (2022). The long non-coding RNA FAM222A-AS1 negatively modulates miR-let-7f to promote colorectal cancer progression. Front. Oncol. *12*, 764621. https://doi.org/10.3389/fonc.2022.764621.
28. Ghosal, S., Saha, S., Das, S., Sen, R., Goswami, S., Jana, S.S., and Chakrabarti, J. (2016). miRepress: modelling gene expression regulation by microRNA with non-conventional binding sites. Sci. Rep. *6*, 22334. https://doi.org/10.1038/srep22334.
29. Senol, O., Schaaij-Visser, T.B.M., Erkan, E.P., Dorfer, C., Lewandrowski, G., Pham, T.V., Piersma, S.R., Peerdeman, S.M., Ströbel, T., Tannous, B., et al. (2015). miR-200a-mediated suppression of non-muscle heavy chain IIb inhibits meningioma cell migration and tumor growth *in vivo*. Oncogene *34*, 1790–1798. https://doi.org/10.1038/onc.2014.120.
30. Zhang, L., Li, S., Choi, Y.L., Lee, J., Gong, Z., Liu, X., Pei, Y., Jiang, A., Ye, M., Mao, M., et al. (2017). Systematic identification of cancer-related long noncoding RNAs and aberrant alternative splicing of quintuple-negative lung adenocarcinoma through RNA-Seq.

Lung Cancer *109*, 21–27. https://doi.org/10.1016/j.lungcan.2017.04.009.
31. Parajón, E., Surcel, A., and Robinson, D.N. (2021). The mechanobiome: a goldmine for cancer therapeutics. Am. J. Physiol. Cell Physiol. *320*, 306–323. https://doi.org/10.1152/ajpcell.00409.2020.
32. Lee, H., Kim, K., Woo, J., Park, J., Kim, H., Lee, K.E., Kim, H., Kim, Y., Moon, K.C., Kim, J.Y., et al. (2018). Quantitative proteomic analysis identifies AHNAK (neuroblast differentiation-associated protein AHNAK) as a novel candidate biomarker for bladder urothelial carcinoma diagnosis by liquid-based cytology. Mol. Cell. Proteomics *17*, 1788–1802. https://doi.org/10.1074/mcp.RA118.000562.
33. Surcel, A., Schiffhauer, E.S., Thomas, D.G., Zhu, Q., DiNapoli, K.T., Herbig, M., Otto, O., West-Foyle, H., Jacobi, A., Kräter, M., et al. (2019). Targeting mechanoresponsive proteins in pancreatic cancer: 4-hydroxyacetophenone blocks dissemination and invasion by activating MYH14. Cancer Res. *79*, 4665–4678. https://doi.org/10.1158/0008-5472.CAN-18-3131.
34. Pérez-Valencia, J.A., Prosdocimi, F., Cesari, I.M., da Costa, I.R., Furtado, C., Agostini, M., and Rumjanek, F.D. (2018). Angiogenesis and evading immune destruction are the main related transcriptomic characteristics to the invasive process of oral tongue cancer. Sci. Rep. *8*, 1–18. https://doi.org/10.1038/s41598-017-19010-5.
35. Golomb, E., Ma, X., Jana, S.S., Preston, Y.A., Kawamoto, S., Shoham, N.G., Goldin, E., Conti, M.A., Sellers, J.R., and Adelstein, R.S. (2004). Identification and characterization of nonmuscle myosin II-C, a new member of the myosin II family. J. Biol. Chem. *279*, 2800–2808. https://doi.org/10.1074/jbc.M309981200.
36. Subramanian, M., Li, X.L., Hara, T., and Lal, A. (2015). A biochemical approach to identify direct microRNA targets. Methods Mol. Biol. *1206*, 29–37. https://doi.org/10.1007/978-1-4939-1369-5_3.
37. Havens, M.A., Reich, A.A., Duelli, D.M., and Hastings, M.L. (2012). Biogenesis of mammalian microRNAs by a non-canonical processing pathway. Nucleic Acids Res. *40*, 4626–4640. https://doi.org/10.1093/nar/gks026.
38. Stavast, C.J., and Erkeland, S.J. (2019). The non-canonical aspects of microRNAs: many roads to gene regulation. Cells *8*, 1465. https://doi.org/10.3390/cells8111465.
39. Duan, Y., Veksler-Lublinsky, I., and Ambros, V. (2022). Critical contribution of 3′ non-seed base pairing to the *in vivo* function of the evolutionarily conserved let-7a microRNA. Cell Rep. *39*, 110745. https://doi.org/10.1016/j.celrep.2022.110745.
40. He, S., Su, H., Liu, C., Skogerbø, G., He, H., He, D., Zhu, X., Liu, T., Zhao, Y., and Chen, R. (2008). MicroRNA-encoding long non-coding RNAs. BMC Genom. *9*, 236. https://doi.org/10.1186/1471-2164-9-236.
41. McGeary, S.E., Bisaria, N., Pham, T.M., Wang, P.Y., and Bartel, D.P. (2022). MicroRNA 3′-compensatory pairing occurs through two binding modes, with affinity shaped by nucleotide identity and position. Elife *11*, 69803. https://doi.org/10.7554/eLife.69803.
42. Thorne, J.L., Battaglia, S., Baxter, D.E., Hayes, J.L., Hutchinson, S.A., Jana, S., Millican-Slater, R.A., Smith, L., Teske, M.C., Wastall, L.M., and Hughes, T.A. (2018). MiR-19b non-canonical binding is directed by HuR and confers chemosensitivity through regulation of P-glycoprotein in breast cancer. Biochim. Biophys. Acta. Gene Regul. Mech. *1861*, 996–1006. https://doi.org/10.1016/j.bbagrm.2018.08.005.
43. Grimson, A., Farh, K.K.H., Johnston, W.K., Garrett-Engele, P., Lim, L.P., and Bartel, D.P. (2007). MicroRNA targeting specificity in mammals: determinants beyond seed pairing. Mol. Cell *27*, 91–105. https://doi.org/10.1016/j.molcel.2007.06.017.
44. Zhai, K.F., Duan, H., Shi, Y., Zhou, Y.R., Chen, Y., Zhang, Y.S., Gong, Z.P., Cao, W.G., Wu, J., and Wang, J.J. (2022). miRNAs from Plasma Extracellular Vesicles Are Signatory Noninvasive Prognostic Biomarkers against Atherosclerosis in LDLr-/-Mice. Oxid. Med. Cell. Longev. *2022*, 6887192. https://doi.org/10.1155/2022/6887192.
45. Bryan, D.S., Stack, M., Krysztofiak, K., Cichoń, U., Thomas, D.G., Surcel, A., Schiffhauer, E.S., Beckett, M.A., Khodarev, N.N., Xue, L., et al. (2020). 4-Hydroxyacetophenone modulates the actomyosin cytoskeleton to reduce metastasis. Proc. Natl. Acad. Sci. USA *117*, 22423–22429. https://doi.org/10.1073/pnas.2014639117.
46. Billington, N., Wang, A., Mao, J., Adelstein, R.S., and Sellers, J.R. (2013). Characterization of three full-length human nonmuscle myosin II paralogs. J. Biol. Chem. *288*, 33398–33410. https://doi.org/10.1074/jbc.M113.499848.
47. Ronen, D., Rosenberg, M.M., Shalev, D.E., Rosenberg, M., Rotem, S., Friedler, A., and Ravid, S. (2010). The positively charged region of the myosin IIC non-helical tailpiece promotes filament assembly. J. Biol. Chem. *285*, 7079–7086. https://doi.org/10.1074/jbc.M109.049221.
48. Case, L.B., and Waterman, C.M. (2015). Integration of actin dynamics and cell adhesion by a three-dimensional, mechanosensitive molecular clutch. Nat. Cell Biol. *17*, 955–963. https://doi.org/10.1038/ncb3191.
49. Smith, A.S., Nowak, R.B., Zhou, S., Giannetto, M., Gokhin, D.S., Papoin, J., Ghiran, I.C., Blanc, L., Wan, J., and Fowler, V.M. (2018). Myosin IIA interacts with the spectrin-actin membrane skeleton to control red blood cell membrane curvature and deformability. Proc. Natl. Acad. Sci. USA *115*, 4377–4385. https://doi.org/10.1073/pnas.1718285115.
50. Croset, M., Pantano, F., Kan, C.W.S., Bonnelye, E., Descotes, F., Alix-Panabières, C., Lecellier, C.H., Bachelier, R., Allioli, N., Hong, S.S., et al. (2018). miRNA-30 family members inhibit breast cancer invasion, osteomimicry, and bone destruction by directly targeting multiple bone metastasis–associated genes. Cancer Res. *78*, 5259–5273. https://doi.org/10.1158/0008-5472.CAN-17-3058.
51. Halder, D., Saha, S., Singh, R.K., Ghosh, I., Mallick, D., Dey, S.K., Ghosh, A., Das, B.B., Ghosh, S., and Jana, S.S. (2019). Nonmuscle myosin IIA and IIB differentially modulate migration and alter gene expression in primary mouse tumorigenic cells. Mol. Biol. Cell *30*, 1463–1476. https://doi.org/10.1091/mbc.E18-12-0790.
52. Gorelik, R., and Gautreau, A. (2014). Quantitative and unbiased analysis of directional persistence in cell migration. Nat. Protoc. *9*, 1931–1943. https://doi.org/10.1038/nprot.2014.131.
53. Zhao, D., Tao, W., Li, S., Chen, Y., Sun, Y., He, Z., Sun, B., and Sun, J. (2021). Apoptotic body–mediated intercellular delivery for enhanced drug penetration and whole tumor destruction. Sci. Adv. *7*, eabg0880. https://doi.org/10.1126/sciadv.abg0880.
54. Kajiwara, C., Fumoto, K., Kimura, H., Nojima, S., Asano, K., Odagiri, K., Yamasaki, M., Hikita, H., Takehara, T., Doki, Y., et al. (2018). p63-dependent Dickkopf3 expression promotes esophageal cancer cell proliferation via CKAP4. Cancer Res. *78*, 6107–6120. https://doi.org/10.1158/0008-5472.CAN-18-1749.
55. Venturi, A., Piaz, F.D., Giovannini, C., Gramantieri, L., Chieco, P., and Bolondi, L. (2008). Human hepatocellular carcinoma expresses specific PCNA isoforms: an *in vivo* and *in vitro* evaluation. Lab. Invest. *88*, 995–1007. https://doi.org/10.1038/labinvest.2008.50.
56. Jana, S.S., Kawamoto, S., and Adelstein, R.S. (2006). A specific isoform of nonmuscle myosin II-C is required for cytokinesis in a tumor cell line. J. Biol. Chem. *281*, 24662–24670. https://doi.org/10.1074/jbc.M604606200.
57. Liang, C.C., Park, A.Y., and Guan, J.L. (2007). *In vitro* scratch assay: a convenient and inexpensive method for analysis of cell migration *in vitro*. Nat. Protoc. *2*, 329–333. https://doi.org/10.1038/nprot.2007.30.
58. Xu, R., Greening, D.W., Zhu, H.J., Takahashi, N., and Simpson, R.J. (2016). Extracellular vesicle isolation and characterization: toward clinical application. J. Clin. Invest. *126*, 1152–1162. https://doi.org/10.1172/JCI81129.

STAR★METHODS

KEY RESOURCES TABLE

REAGENT or RESOURCE	SOURCE	IDENTIFIER
Antibodies		
Anti-NMHC-IIA antibody	Sigma / Cell Signaling Technology	Cat# M8064 and Cat# 3403
Anti-NMHC-IIB antibody	Sigma and Cell Signaling Technology	Cat# M7939 and Cat# 3404
Anti-NMHC-IIC antibody	Sigma	Cat# SAB4503174
Anti-GFP antibody	Sigma	Cat# G1544
Anti-AGO2 antibody	Cell Signaling Technology	Cat# 2897
Anti-GAPDH antibody	Santa Cruz	Cat# sc-32233
Anti-PCNA antibody	Santa Cruz	Cat # sc-56
Alexa Fluor 594-conjugated anti rabbit secondary antibody	ThermoFisher	Cat# A-11012
Chemicals, peptides, and recombinant proteins		
Lipofectamine 2000	ThermoFisher	Cat# 11668019
Dapi	Sigma	Cat# D8417
Alexa Fluor 488-conjugated phalloidin	ThermoFisher	Cat# A12379
Prolong gold antifade reagent	ThermoFisher	Cat# P36965
SureBeads Protein G Magnetic Beads	BioRad	Cat# 1614021
Dynabeads M-280 Streptavidin	ThermoFisher	Cat # 11205D
Critical commercial assays		
Dual luciferase assay kit	Promega	Cat# E1910
MystiCq® MicroRNA® Quantitation System	Merck	Cat# MIRRT
mirVana™ miRNA Isolation Kit	ThermoFisher	Cat# AM1560
RNeasy Mini Kit	Qiagen	Cat# 74004
Mouse specific horseradish peroxidase (HRP)/3,3′-diaminobenzidine (DAB) (ABC) Detection IHC Kit	Abcam	Cat# ab64259
Experimental models: Cell lines		
4T1	ATCC	ATCC-CRL-2539
Neuro2a	ATCC	ATCC-CCL-131
HEK293	ATCC	ATCC-CRL-1573
MCF7	ATCC	ATCC-HTB-22
MDA-MB231	ATCC	ATCC HTB-26
Oligonucleotides		
Non-specific mimic miRNA	Sigma	Cat# HMC0003
Non-specific miRNA inhibitor	ThermoFisher	Cat# 4464076
mmu-miR-200a-5p	Qiagen	This manuscript
mmu-miR-532-3p	Qiagen	This manuscript
mmu-miR-680	Qiagen	This manuscript
mmu-miR-1901	Qiagen	This manuscript
Anti-miR-200a-5p	Sigma	This manuscript
Anti-miR-532-3p	Sigma	This manuscript
Anti-miR-680	Sigma	This manuscript
Anti-miR-1901	Sigma	This manuscript
Biotin-non-specific miRNA	Qiagen	This manuscript

(*Continued on next page*)

Continued

REAGENT or RESOURCE	SOURCE	IDENTIFIER
Biotin-miR532-3p	Qiagen	This manuscript
Non-specific siRNA	Sigma	Cat# SIC001
siRNA against the 3′UTR region of MYH14	Sigma	5′-UUGAACGUGGAUGUCAAGA-3′and 5′-UCUUGACAUCCACGUUCAA-3′
Forward primer for Myh9	Sigma	5′-CCAGAAGCCCAAGCAACTGAA-3′
Reverse Primer for Myh9	Sigma	5′-AGGCACCAGGTAGTGCTGTCT-3′
Forward primer for Myh10	Sigma	5′-TCAGAAGCCGCGCCAACTGAA-3′
Reverse primer for Myh10	Sigma	5′-ATGCAGAGCCAAACGCGGTCT-3′
Forward primer for Myh14	Sigma	5′-AGACAGGCCAAGGATGAATG-3′
Reverse primer for Myh14	Sigma	5′CCATTGGTCAGGAAGCGATAA-3′
Forward primer for MYH14	Sigma	5′-ATGCTGCAGGATCGTGAGGACC-3′
Reverse primer for MYH14	Sigma	5′-ATGAATTTGCCGAATCGGGAGG-3′
Forward primer for GAPDH (mouse)	Sigma	5′-GACAACTTTGGCATTGTGGAA-3′
Reverse primer for GAPDH (mouse)	Sigma	5′-ACACATTGGGGGTAGGAACA-3′
Forward primer for GAPDH (human)	Sigma	5′-GAGTCAACGGATTTGGTCGT-3′
Reverse primer for GAPDH (human)	Sigma	5′-TTGATTTTGGAGGGATCTCG-3′
Primer for miR-200a-5p	Sigma	5′-CATCTTACCGGACAGTGCTGGA-3′
Primer for miR-532-3p	Sigma	5′-CCTCCCACACCCAAGGCTTGCA-3′
Primer for miR-680	Sigma	5′-GGGCATCTGCTGACATGGGGG-3′
Primer for miR-1901	Sigma	5′-CCGCTCGTACTCCCGGGGGTCC-3′
Primer for U6 (mouse)	Sigma	5′-TGGCCCCTGCGCAAGGATG-3′
Recombinant DNA		
WT 3′UTRs of NMHC-IICmRNA tagged firefly luciferase plasmid DNA	N/A	This manuscript
MT 3′UTRs of NMHC-IICmRNA tagged firefly luciferase plasmid DNA	N/A	This manuscript
Renilla luciferase plasmid DNA		N/A
NMIIC-GFP		N/A
NMIIA-mCherry		N/A
NMIIB-mCherry		N/A
Software and algorithms		
Fiji	NIH	https://fiji.sc/
Zen Blue	Zeiss	N/A
GraphPad Prism 8	GraphPad Software Inc.	https://www.graphpad.com

RESOURCE AVAILABILITY

Lead contact

Further information and requests for resources and reagents should be directed to and will be fulfilled by the lead contact, Siddhartha S Jana (bcssj@iacs.res.in).

Materials availability

The new reagents generated in this study are available from the lead contact with a completed Materials Transfer Agreement.

Data and code availability

- Data reported in this paper will be shared by the lead contact upon request.
- This paper does not report any original code.
- Any additional information required to reanalyse the data reported in this paper is available from the lead contact upon request.

EXPERIMENTAL MODEL AND STUDY PARTICIPANT DETAILS

Cell lines

Mouse breast cancer 4T1 cells and neuroblast Neuro-2a cells were procured from American Type Culture Collection (ATCC) and were maintained as per their guidelines. Briefly, 4T1 and Neuro-2a cells were grown in RPMI-1640 and DMEM, respectively, supplemented with 10% FBS and 100 μg/ml Penicillin/Streptomycin at 37°C in a humidified chamber in the presence of 5% CO_2. Human HEK293, MCF7, MDA MB-231 cells were also procured from American Type Culture Collection (ATCC) and were maintained as per their guidelines. We have not performed any authentication as the cells were already authenticated by ATCC. All the cell lines were routinely tested for mycoplasma contamination in the laboratory. Briefly, HEK293 and MCF7 cells were grown in DMEM and MDA MB-231 cells in L-15, supplemented with 10% FBS and 100 μg/ml Penicillin/Streptomycin. Cells were maintained at 37°C in a humidified chamber in the presence of 5% CO_2 (except MDA MB-231).

Laboratory animals

Six to eight-week- old female BALB/c mice were procured from the State Centre for Laboratory Animal Breeding (SCLAB, WBLDCL, Kalyani, India) and all the animal experiments were carried out according to the guidelines of the Institutional Animal Ethics Committee of Indian Association for the Cultivation of Science, Kolkata.

METHOD DETAILS

miRNA and plasmid DNA transfection

Approximately, $5x10^5$ 4T1 cells were transfected with 40-60 nM mimic miRNA,miRNA inhibitor, or non-specific (NS) mimic miRNA (HMC0003, Sigma, St. Louis, USA), or NS mirVana™ miRNA inhibitor (4464076, ThermoFisher, Waltham, USA) oligos only, or co- transfected with the miRNA oligos, 500 ng WT or mutant 3′UTRs of NMHC-IICmRNA tagged firefly luciferase, and 100 ng renilla luciferase plasmid DNAs, or co-transfected with 40-60 nM mimic or inhibitor of miR-532-3p, and 1 μg GFP tagged NMHC-IIC, and mCherry tagged NMHC-IIA or NMHC-IIB using Lipofectamine™ 2000 (ThermoFisher). 5x105 HEK293 cells were co-transfected with 40-60 nM mimic of miRNA and 1 μg GFP tagged CDS of NMHC-IIC mRNA to check the exogenous level of NMHC-IIC. The cells were analyzed at 72h post transfection. GFP and mCherry were visualized using Carl Zeiss LSM880 confocal microscope (Zeiss, Germany) equipped with Zen Blue Software. GFP alone encoding plasmid DNA was used to measure the transfection efficiency of plasmid DNAs, which was above 60%.

SiRNA transfection

Approximately, $5x10^5$ 4T1 cells were transfected with 40 nM of non specific (NS siRNA, #SIC001, Sigma) or specific siRNA targeting the 3′UTR region using Lipofectamine™ 2000 ThermoFisher).

Bioinformatics analysis

We searched for potential canonical and non-canonical miRNAs against NMHC-IICmRNA in mouse breast cancer cell lines following a previously published method, miRepress (Release miRepress_mouse suman-ghosal/miRepress (github.com).[28] The miRNAs were ranked based on their miRepress score and their ability to bind both at canonical and non-canonical sites. We changed the miRNA seed region definition in each case for the prediction of different types of miRNA target sites (6-mer, 7-mer, 7-merA1 and 8-mer). We considered transcripts with perfect seed complementarity as well as one base mismatch tolerance in the seed region with 3′ compensatory complementarity. For canonical miRNA binding sites, the miRNA seed region is defined as the base position 2-7 from the 5′ end of the miRNA, and for non-canonical binding sites, the miRNA seed region is defined as position 2-7 from the 3′ end of the miRNA. Targets were searched in the 5′ untranslated region, coding sequence and 3′ untranslated region of protein-coding genes. The miRepress score was calculated based on the number of canonical and non-canonical target sites. We used Cytoscape to assess other targets of the top four miRNAs, apart from Myh14. We also used Gene ontology biological process enrichment analysis to predict pathways in which the miRNAs, miR-200a-5p, miR-532-3p, miR-1901 and miR-680 mediated gene expression are involved. The most enriched pathways were sorted according to their enrichment p-value.

Dual luciferase assay

The dual-luciferase assay was carried out according to the previously published protocol.[50] Briefly, at 72h, ~$5x10^5$ 4T1 cells co-transfected with 40-60 nM mimic or inhibitor of miRNA, and 500 ng of firefly luciferase tagged WT or mutant 3′UTRs of NMHC-IICmRNA, and 100 ng of renilla luciferase plasmid DNAs were lysed for detecting firefly luciferase signal using dual luciferase assay kit (Promega). The signal was recorded in a luminometer, Luminoskan™ Microplate Luminometer (ThermoFisher). Renilla luciferase was used as an internal control to normalize the firefly luciferase signal. Fold changes in luminescence signal by each of the mimic or inhibitor miRNA oligos were calculated by considering normalized luminescence value from NS RNA oligos (mimic or inhibitor) treated cells as "1".

Immunoprecipitation, immunoblot and SDS-PAGE

Immunoprecipitation (IP) of NMHC-IIs was performed using SureBeads Protein G Magnetic Beads (BioRad, Hercules, USA) as per manufacturer's protocol. Briefly, ~ $1x10^7$ cells were lysed in buffer A composed of 50 mM Tris-HCl (pH 8.0), 150 mM NaCl, 10 mM $MgCl_2$, 5 Mm ATP, 10 mM EDTA, 1 mM dithiothreitol, 1% NP-40, 0.5 mM PMSF, and protease inhibitor cocktail (Sigma), at 4°C. Cell lysates were sonicated and

centrifuged at 12,000×g for 15 min at 4°C. A 3000 μg cell lysate was incubated with 10μg of magnetized antibody beads at rt for 1 h.[51] For magnetization, 100μl of protein G magnetic beads suspension were washed and noncovalently complexed with 10μg NMHC-IIA or -IIB antibody (Cell Signaling Technology, Danvers, USA). Only protein G magnetic beads were used as negative control for IP reaction. The beads were collected and the immunocomplexes were eluted in 2x Laemmli Buffer. The cell lysates or immunocomplexes were resolved on 10% SDS-PAGE, and transferred to PVDF membrane, and blocked with 5% non-fat skim milk at rt for 1 h. The membranes were incubated with antibodies against NMHC-IIA, -IIB, -IIC (1:2000, Sigma), GFP (1:2000, Sigma), GAPDH (1:4000, Santa Cruz, Dallas, USA) or AGO2 (1:2000, Cell Signaling Technology) at 4°C for overnight. The blots were washed with PBS containing 0.05% Tween-20 and incubated with HRP-conjugated mouse or human secondary antibodies at rt for 2 h. SuperSignal™ West Femto maximum sensitivity substrate (ThermoFisher) was used to generate luminescence signal which was captured using a ChemiDoc™ Touch Imaging System (BioRad).

RNA isolation, cDNA preparation and qRTPCR

Total RNA was isolated from mouse spleen and lung tissues, or 4T1 cells, which were transfected with or without mimic or inhibitor miRNA oligos, using the RNeasy Mini Kit (Qiagen, Hilden, Germany). The cDNA was synthesized using First Strand cDNA Synthesis Kit (Roche, Basel, Switzerland), and amplified using ReadyMix™ Taq PCR Reaction Mix (Sigma) and primers specific to Myh9, Myh10 and Myh14. Products generated by RT-PCR were electrophoresed in a 1.8% agarose (Lonza, Basel, Switzerland) gel and the bands were visualized by EtBr staining. GAPDH was used as the internal reference. Similarly, small RNA isolation, c-DNA synthesis and its quantification by quantitative PCR were carried out according to the manufacturer's protocol (MystiCq® MicroRNA® Quantitation System (Merck, Rahway, USA) or mirVana™ miRNA Isolation Kit (ThermoFisher). Briefly, small RNAs were first isolated from different tissues and cell lines using RNAzol® RT and then polyadenylated with poly A polymerase. The poly (A) tailed small RNAs were then subsequently converted into first-strand cDNA using ReadyScript Reverse Transcriptase and an oligo-dT adapter primer. Next, miRNA cDNAs were amplified using the MystiCq microRNA qPCR Universal Primer and individual miRNA primers. PCR Products were electrophoresed in a 2% agarose gel and the bands were visualized by EtBr staining. U6 was used as the internal reference to normalize the miRNA gene levels.

Biotin-miR-532-3p pulldown assay

Biotin-labeled miR-532-3p pulldown assay was carried out according to the previously published protocol.[36] Briefly, biotin-miR532-3p or biotin-non-specific miRNA was co-transfected with WT or each of MTs 3′UTR of NMHC-IICmRNA in $5x10^5$ 4T1 cells. At 24h post transfection, the cells were lysed with a lysis buffer [20 mM Tris–HCl (pH 7), 100 mM KCl, 5 mM $MgCl_2$, 0.3% NP-40] for 20 min. The cell lysate was incubated with Dynabeads M-280 Streptavidin (ThermoFisher) for 4h and subsequently, washed with lysis buffer. The bound miRNA-RNA complexes in each sample were eluted using the lysis buffer supplemented with 0.1% SDS and 500 μg/ml proteinase K at 55°C for 20 min. The amount of bound NMHC-IICmRNA was determined by qRTPCR method as applied before.[36] Fold was calculated by following $2^{-\Delta\Delta Ct}$ method, where ΔΔCT=ΔCT mimic miRNA - ΔCT NS miRNA. ΔCT is the difference between CT values of the NMHC-IIC and GAPDH mRNAs.

Soft agar colony assay

A base layer was prepared with 0.5% agar in RPMI-1640 complete growth medium (GM) and kept at 37°C for 1h in a 35 mm culture dish. Mimic, NS mimic, NS inhibitor or inhbitor of miRNA transfected 4T1 cells were suspended in GM containing 0.3% agarose and plated on the base layer. Cells were allowed to grow for 14 days in an incubator at 37°C in the presence of 5%CO_2. The formation of colonies and their growth were monitored by capturing images at seven days intervals using a bright field microscope (Nikon, Tokyo, Japan). Areas of the colonies were quantified using Fiji software (NIH, USA).

Cell migration and live cell imaging

The 4T1 cells were transfected with mimic, NS mimic, NS inhibitor or inhbitor miRNA. At 72h cells were tracked by capturing images at 5min intervals for 12h using a CCD camera (Digital Sight DS-Qi1MC, Nikon) in a live cell incubator at 37°C supplied with 5%CO_2. Movies were played at a speed of 10fps. The center of each cell in the image sequence was manually analyzed by Fiji software (NIH). Average speed and cell trajectory were calculated using a published protocol, DiPer.[52] Cell migration through a Boyden chamber (CLS 3464, Corning) was performed using the manufacturer's protocol. Briefly, transwell inserts were placed in 24- well plates. 100μl of 4T1 cells suspension ($4×10^5$ cells/ml), which were previously transfected with mimic or anti miRNA oligos (inhibitor), were added to the upper chamber of each insert in serum free medium whereas only cell-free medium supplemented with 10%FBS was added to the lower chamber. The setup was kept at 37°C and 5%CO_2 conditions in a humidified incubator. At 24h, the upper surface of the transwell insert was carefully cleansed with cotton pads to remove non migrated cells, and the migrated cells at bottom surface were stained with crystal violet (Sigma) for 15min. The images were captured at 8X objective using a stereo microscope (Nikon). The number of migrated cells per field was counted using the Fiji software.

Cytoskeletal fractionation

Cytoskeletal fractionation with TX-100 extraction buffer was carried out following a published protocol.[49] Approximately $2×10^7$ cells were transfected with NS miRNA or mimic miR-532-3p or inhibitor miR-532-3p oligos. At 72h post transfection, cell lysates were prepared using 500 μl of ice-cold TX-100 extraction buffer composed of 10mM $NaHPO_4$ (pH 7.5), 0.2% TX-100, 2mM $MgCl_2$, 1mM EGTA, 1mM DTT, 5mM

ATP, cocktail of protease and phosphatase inhibitors (Sigma), and incubated on ice for 5 min. The lysates were centrifuged at 21,000×g at 4°C to sediment the TX-100 insoluble skeletons. The supernatant (soluble fraction) was collected, and the pellet (insoluble fraction) was resuspended with extraction buffer. Both the soluble and insoluble fractions were analyzed for NMII paralogs by immunoblot analyses.

In vivo tumor formation in mice and immunohistochemistry

Approximately, $1x10^5$ 4T1 cells which were previously transfected with mimic or anti-miRNA oligos were subcutaneously injected in hind leg of mice according to a published protocol.[53] Tumor bulge was visible in mice within 10-13 days. On 32nd day, the mice were sacrificed and tumor tissues were collected. Tumor length (L) and width (W) were measured using calipers, and tumor volume (V) was calculated following the equation, V = (L x W2)/2.[54] Tumor tissues were fixed in 10% formalin solution overnight. Paraffin-embedded tissue sections were prepared for hematoxylin and eosin staining (H&E). Paraffin-embedded tissue sections, next to a H&E section, were prepared for immunohistochemistry. Briefly, deparaffinized and rehydrated sections were subjected to antigen retrieval in 10 mM sodium citrate (pH 6) for 20 min at 80°C.[55] Sections were then permeabilized with 0.1% Triton X-100 and blocked with normal goat serum followed by incubation with primary antibody against PCNA (dilution- 1:300, Santa Cruz). Next, the samples were immunostained using Mouse specific HRP/DAB (ABC) Detection IHC Kit as per the manufacturer's protocol (ab64259, Abcam, Cambridge, UK). Images were captured using a BX53M microscope (Olympus, Tokyo, Japan).

Cloning of 3/UTR and CDS of NMHC-II mRNA

The 3′UTR of NMHC-IICmRNA (NM_001271538; 6108 to 6515) was picked up from the genomic DNA of mouse Neuro-2a cells using primers, FP1, 5′- GGTACCGGATCCTCCAGTCTGTCCTAGATGC-3′ and RP1, 5′-GCGGCCGCCTCGAGTGAAGGGTCCAGCCAGTTTAT-3′ and cloned at BamHI and NotI sites of a firefly luciferase vector, PCDNA3.1. The PCR cycle was programmed for 5 min at 95°C as initial denaturation, followed by 39 cycles of 30 sec at 95°C for denaturation, 30 sec at 55°C as annealing, 45 sec at 72°C for extension, and final extension at 72°C for 5 min. The mutants at 3′UTR (substitution of GG with AA at +162 and GC with AA at +251) were incorporated using the following set of primers- FP2: 5′- GCACCTATTTTCAGCAGAACTGTCCCCTGGAGAGG-3′, RP2: 5′- CCTCTCCAGGGGACAGTTCTGCTGAAAATA GGTGC-3′, and FP3: 5′-CCAAACCAAGGAGCTGGGTAAGAGGGAGGCCATGATGGTC-3′, RP3: 5′-GACCATCATGGCCTCCCTCTTACC CAGCTCCTTGGTTTGG-3′, respectively, using site directed mutagenesis. The PCR was carried out with WT-3′UTR-pcDNA3.1 as template DNA using Pfu DNA Polymerase (Promega, Madison, USA). The PCR product was digested with DpnI enzyme for 3 h at rt to eliminate the template DNA, and transformed into DH5α cells. Substitutions of GG and GC with AA in the 3′UTR-pcDNA3.1 plasmids were confirmed by sequencing. The plasmid DNA encoding GFP tagged CDS of NMHC-IIC[56] was amplified and all the plasmid DNAs were transfected to 4T1 cells using Lipofectamine™ 2000.

Immunofluorescence confocal microscopy

Briefly, 4T1 cells were transfected with mimic or inhibitors of miRNAs. At 72 h post transfection, the cells were washed in PBS and fixed in 4% paraformaldehyde for 15 min. Next, permeabilization was performed using 0.5% Triton X-100 for 10 min. Subsequently, the cells were incubated with 3% BSA for 60 minutes followed by antibody against NMHC-IIA (Sigma) at 4°C overnight. Then, Alexa Fluor 594-conjugated anti rabbit secondary antibody (Thermo Fisher) and Alexa Fluor 488-conjugated phalloidin (Thermo Fisher) were added at 1:1000 dilutions, and incubated for 60 min. The nuclei were stained with DAPI. Coverslips were mounted using Prolong gold antifade reagent (Thermo Fisher). Images were captured using Carl Zeiss LSM880 confocal microscope (Zeiss, Germany) equipped with Zen Blue software.

Would healing assay

For wound healing assay, 4T1 cells transfected with mimic or anti miRNA oligos were allowed to grow in a monolayer in the presence of complete growth medium. At 72 h post transfection when the cell-confluency was almost 90-100%, a scratch-wound was created using a pipette tip according to the previously published protocol.[57] Images of wound areas were captured at 5 mins interval for duration of 12 hours. The wound areas at 3h, 6h, 9h and 9h were then calculated by Fiji Software.

Extracellular vesicle isolation

Extracellular vesicles were isolated according to a published protocol.[58] Briefly, the conditioned medium (CM) of 4T1 cells was centrifuged at 1,000-2000×g for 5 min at 4°C to remove intact cells and debris. The supernatant was centrifuged at 10,000×g for 30 min to collect vesicles of size ~50-1500nm. Isolated pool of extracellular vesicles was washed and resuspended in 30 μl of cold PBS. 5 μL of the suspension was drop-casted on glass plates and gold spattering was done for 90 sec before capturing the images. The images were captured using a JEOL-JSM-7500F field-emission scanning electron microscope to visualize the vesicles, and the rest supernatant was used for small RNA isolation.

Total RNA isolation from human tissues, cDNA preparation and qRTPCR

All experimental procedures were approved by the Ethical Committee of Institute of Post Graduate Medical Education and Research (IPGMER), Kolkata, and Indian Association for the Cultivation of Science. Both tumor (T) tissue and normal tissue associated with tumor (NTAT) obtained at the time of surgery from colon and gastric cancer, and contralateral sarcoma patients who were admitted to IPGMER, Kolkata, and immediately stored at -80°C. All patients provided written consent for the use of these clinical samples in the research work.

Total RNA was isolated from the tissues using the RNeasy Mini Kit (Qiagen, Hilden, Germany). The cDNA was synthesized using First Strand cDNA Synthesis Kit (Roche, Basel, Switzerland), and amplified using ReadyMix™ Taq PCR Reaction Mix (Sigma) and primers specific to MYH14. Quantitative PCR was carried out with QuantiTect SYBR Green qPCR Mix (Qiagen) to quantify the relative amount of MYH14. GAPDH was used as the internal reference. The relative values of MYH14 were calculated using $2^{-\Delta\Delta Ct}$ method, where ΔΔCT= ΔCT(T) – ΔCT(NTAT). ΔCT is the difference between CT values of the MYH14 and GAPDH mRNA. Similarly, small RNA isolation, c-DNA synthesis and its quantification by quantitative PCR were carried out according to the manufacturer's protocol (MystiCq® MicroRNA® Quantitation System (Merck, Rahway, USA) or mirVana™ miRNA Isolation Kit (ThermoFisher). The relative abundance of miRNAs was calculated by the $2^{-\Delta\Delta Ct}$ method, where ΔΔCT= ΔCT(T) – ΔCT(NTAT). ΔCT is the difference between CT values of the miRNA and U6.

QUANTIFICATION AND STATISTICAL ANALYSIS

The data are represented as the means ± standard error of the mean (SEM). The statistical significance was analyzed with two-tailed Student's student's t-test when two groups were studied, or one- way ANOVA followed by post hoc Tukey's multiple comparison when more than two groups were studied in the analysis using GraphPad Prism 8 software. A p-value of <0.05 was considered statistically significant and indicated in the figures as *$p < 0.05$, **$p < 0.01$ and ***$p< 0.001$.